Supporting Information

Antibiotic-triggered reversible luminescence switching in amine-grafted mixed-linker MOF: exceptional turn-on and ultrafast nanomolar detection of sulfadiazine and adenosine monophosphate with molecular keypad lock functionality

Ranadip Goswami,[ab] Shyama Charan Mandal,[c] Nilanjan Seal,[ab] Biswarup Pathak,[c] and Subhadip Neogi*[,ab]

[a.]Academy of Scientific and Innovative Research (AcSIR), (CSIR-CSMCRI), Bhavnagar, 364002, Gujarat, India
[b.]Inorganic Materials & Catalysis Division, CSIR-CSMCRI Bhavnagar, Gujarat-364002, India
[c.]Discipline of Chemistry, Indian Institute of Technology (IIT) Indore, Indore, Madhya Pradesh, 453552, India
*E-mail: sneogi@csmcri.res.in

Table of contents

1. Materials and methods

All the reagents employed were commercially available (except *dpta*) and used as provided without further purification. $Zn(NO_3)_2 \cdot 6H_2O$, Azobenzene-4,4'-dicarboxylic Acid (H_2*azdc*), hydrazine monohydrate, 4-cyano pyridine were purchased from Sigma−Aldrich and TCI chemicals, respectively. All the solvents such as HPLC grade N, N′−dimethylformamide (DMF), dichloromethane (DCM), ethanol were procured from either Loba chemie Pvt. Ltd., India or S. D. Fine Chemicals., India. All the antibiotics, biophosphates, used in this study were purchased from TCI chemicals. Linker *dpta* was synthesized according to the reported literature procedure.[1] All spectroscopic and crystallographic studies are provided in the following sections.

Caution!!! Being hazardous in nature, all analytes should be handled carefully.

2. Physical measurements

The infrared spectra (IR) of the samples were recorded using the KBr pellet method on a Perkin–Elmer GX FTIR spectrometer in the region of 400−4000 cm-1. Powder X-ray diffraction (PXRD) data were collected using a PANalytical Empyrean (PIXcel 3D detector) system equipped with Cu K_α (λ=1.54 Å) radiation. Microanalyses of the compounds were conducted using elementar vario MICRO CUBE analyzer. Thermogravimetric analyses (TGA) (heating rate of 5 °C/min under N_2 atmosphere) were performed with a Mettler Toledo Star SW 8.10 system. Prior to all fluorescence experiments, as-synthesized compounds were immersed in dry DCM for 3 days at room temperature to replace lattice guest molecules. The solvent-exchanged frameworks were then degassed overnight under vacuum at 120 °C to generate **2a**. UV-Vis spectra recorded using Shimadzu UV-3101 PC spectrometer and the luminescence experiments were performed at room temperature using a Fluorolog Horiba Jobin Yvon spectrophotometer.

3. X-ray structural studies

Single crystals with suitable dimensions were chosen under an optical microscope and mounted on a glass fibre for data collection. Intensity data for as synthesized orange block crystal of **CSMCRI-2** were collected using graphite-monochromated MoKα (λ=0.71073 Å) radiation on a Bruker SMART APEX diffractometer equipped with CCD area detector at 173 K, The linear absorption coefficients, scattering factors for the atoms, and the anomalous dispersion corrections were taken from International Tables for X-ray Crystallography. The data integration and reduction were performed with SAINT[2] software. Absorption corrections to the collected reflections were accounted with SADABS[3] using XPREP.[4] The structure was solved by direct method using SIR-97[5] and was refined on F2 by the full-matrix least-squares technique using the SHELXL-2014[6] program package. All H atoms were placed in calculated positions using idealized geometries (riding model) and assigned fixed isotropic displacement parameters using the SHELXL default. To give an account of disordered electron densities associated with solvent molecules, the "SQUEEZE" protocol in PLATON[7] was applied that produced a set of solvent free diffraction intensities. Final cycles of least-squares refinements improved both the R values and Goodness of Fit with the modified data set after subtracting the contribution from the disordered solvent molecules, using SQUEEZE program. The crystal and refinement data for **CSMCRI-2** is listed in Table S1. Topological analysis was performed by using TOPOS software.[8]

4. Synthesis of $[Zn_2(azdc)_2(dpta)]\cdot(DMF)_4$ (**CSMCRI-2**)

A mixture of $Zn(NO_3)_2\cdot 6H_2O$ (14.9 mg; 0.05 mmol), azobenzene-4,4′-dicarboxylic acid (H_2azdc) (13.6 mg; 0.05 mmol), and *dpta* (12 mg; 0.05 mmol) was dissolved in 4 mL of DMF that was placed in a 15 mL tightly capped Teflon-lined glass vial and heated under autogenous pressure at 90 °C for 48 h. Block-shaped orange crystals were isolated in 62% yield. The crystals were washed with DMF and finally dried in air. The guest solvents in the as-synthesized crystals were exchanged with dichloromethane and degassed overnight under vacuum at 120 °C to generate a solvent-free framework $[Zn_2(azdc)_2(dpta)]$ (**2a**). Anal. Calcd for $C_{40}H_{26}N_{10}O_8Zn_2$ (**2a**): C, 53.06; H, 2.89; N, 15.47%. Found: C, 53.21; H, 3.03; N, 15.39%.

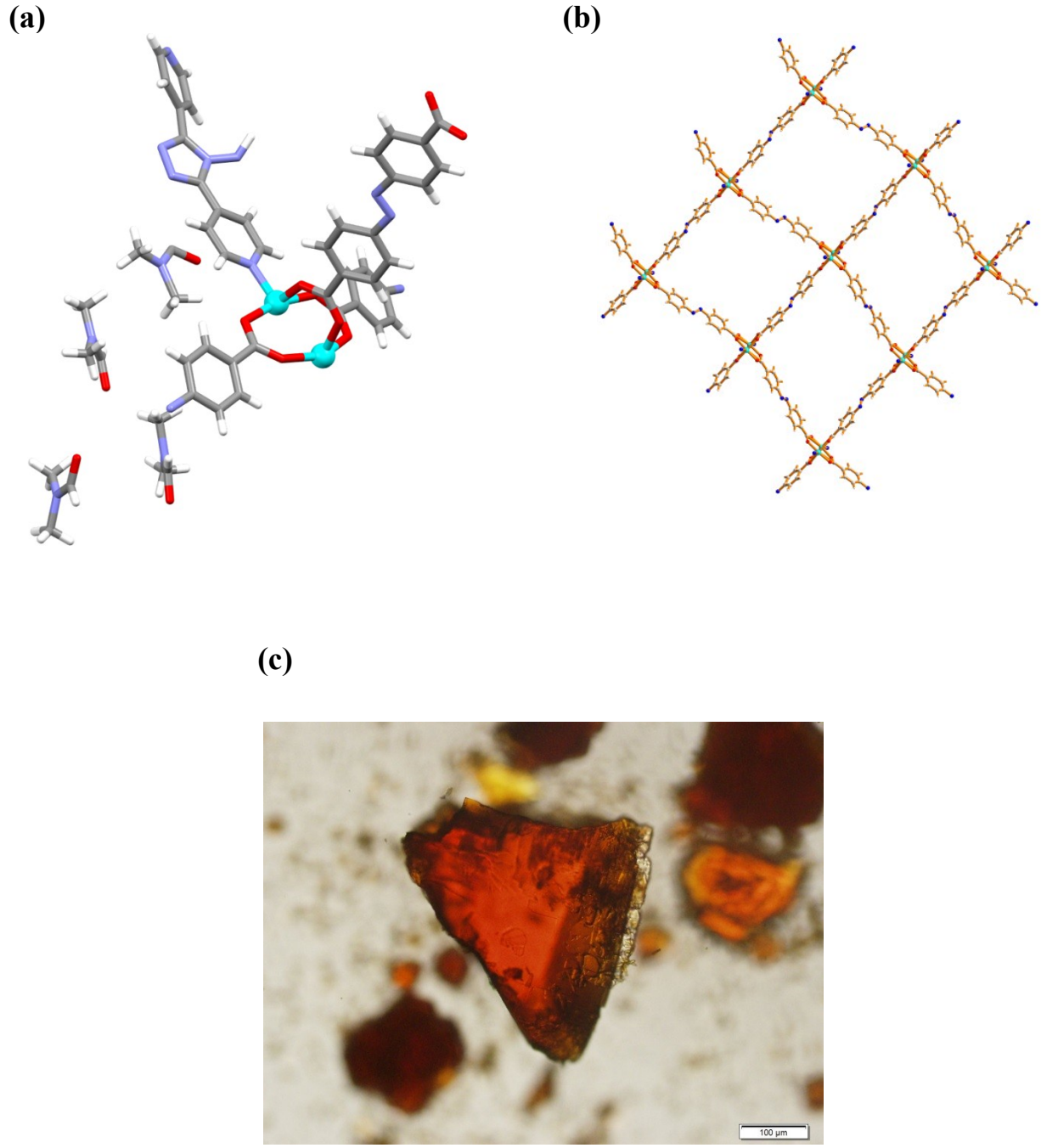

Figure S1. (a) Asymmetric unit of **CSMCRI-2** b) View of the 2-D layer, with paddle-wheel SBUs. (c) Optical microscopic image of **CSMCRI-2**.

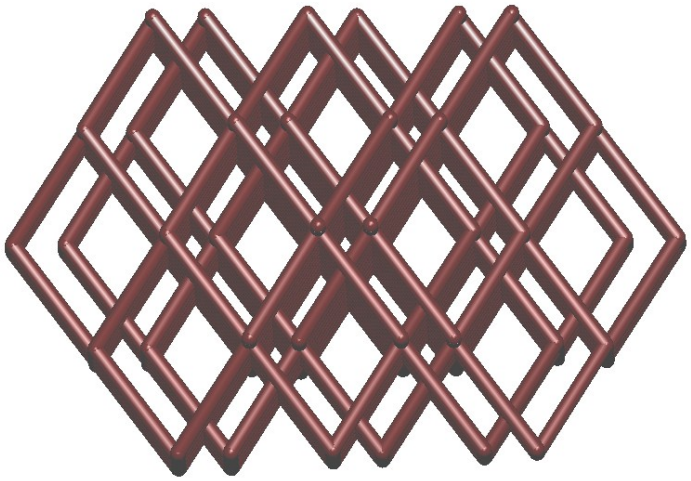

Figure S2. The topology of **CSMCRI-2**, showing 3 (1+2) interpenetrating nets.

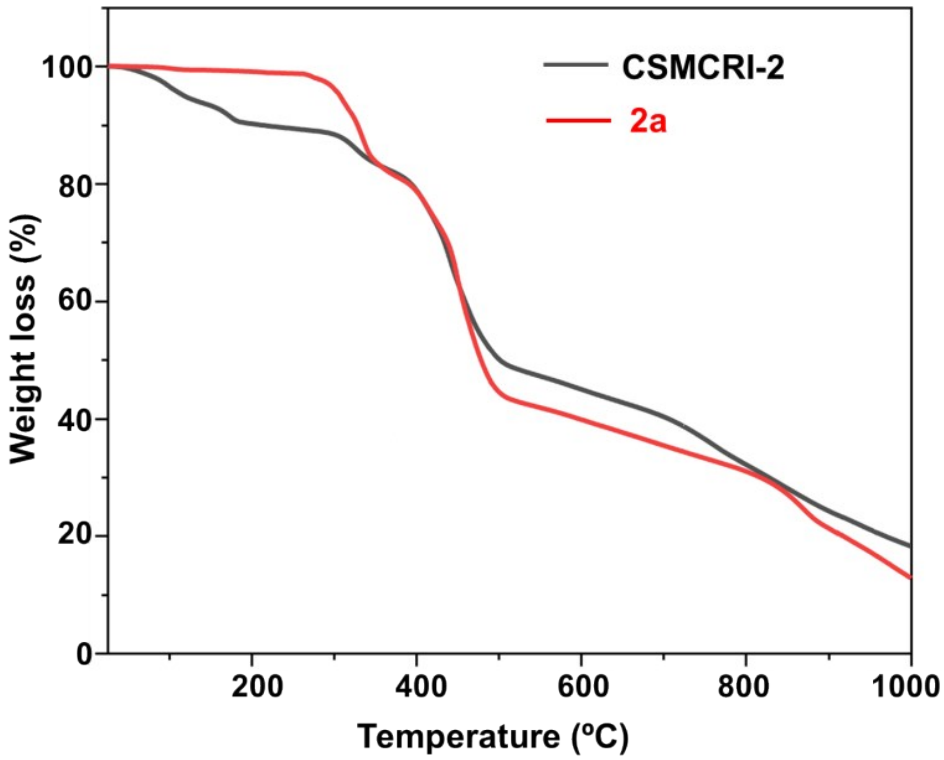

Figure S3. Thermogravimetric analysis of as-made **CSMCRI-2** (black) and after activation (**2a**) (red).

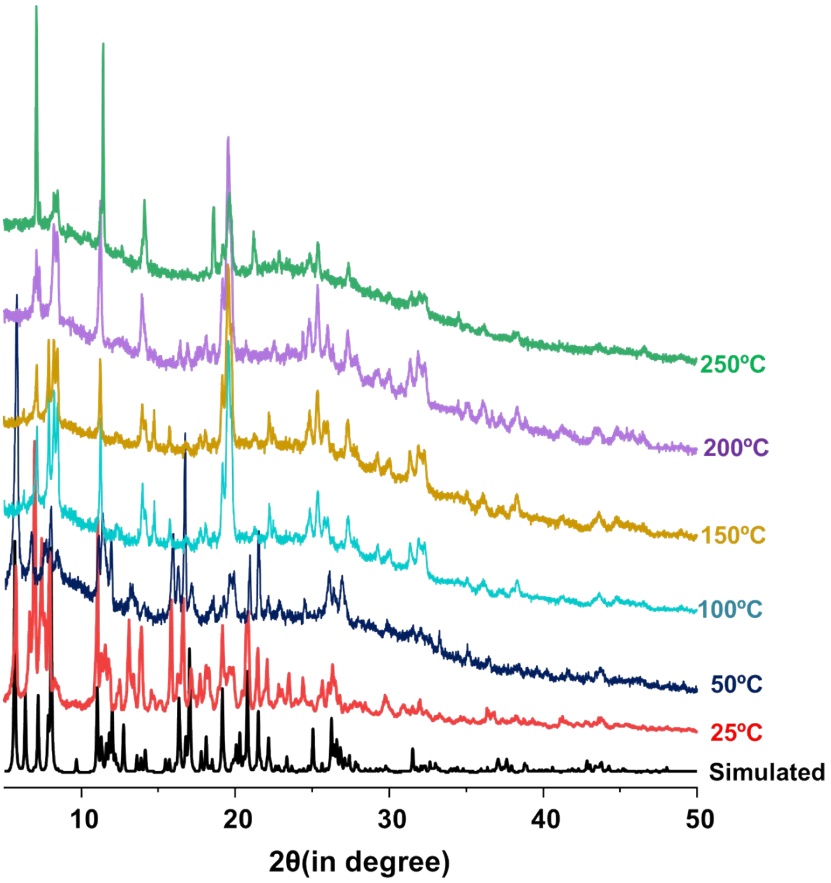

Figure S4. Variable temperature powder X-ray diffraction (VT-PXRD) patterns for **CSMCRI-2**.

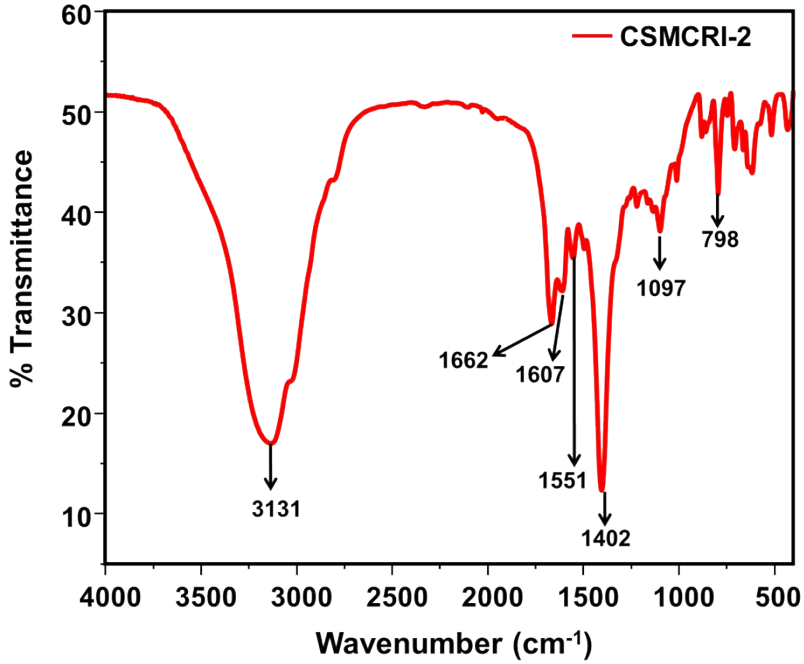

Figure S5. FT-IR spectra (KBr pellets, cm^{-1}) of **CSMCRI-2**.

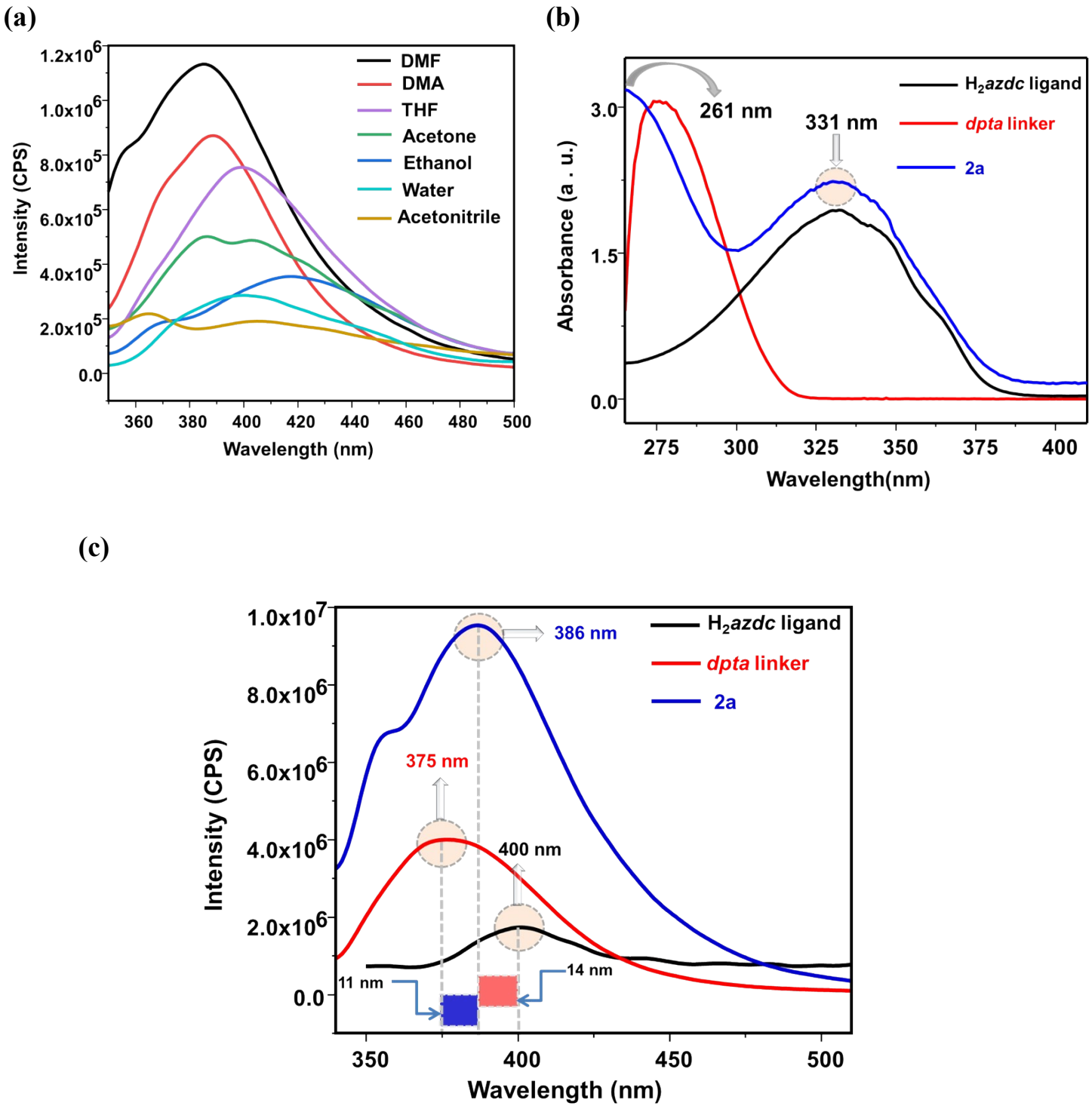

Figure S6. a) Emission intensity of **2a** dispersed in various solvents. b) UV-Vis spectra of constituting ligands of **CSMCRI-2** and **2a**. c) Emission intensity of ligand H_2*azdc*, linker *dpta*, and **2a** (all dispersed in DMF).

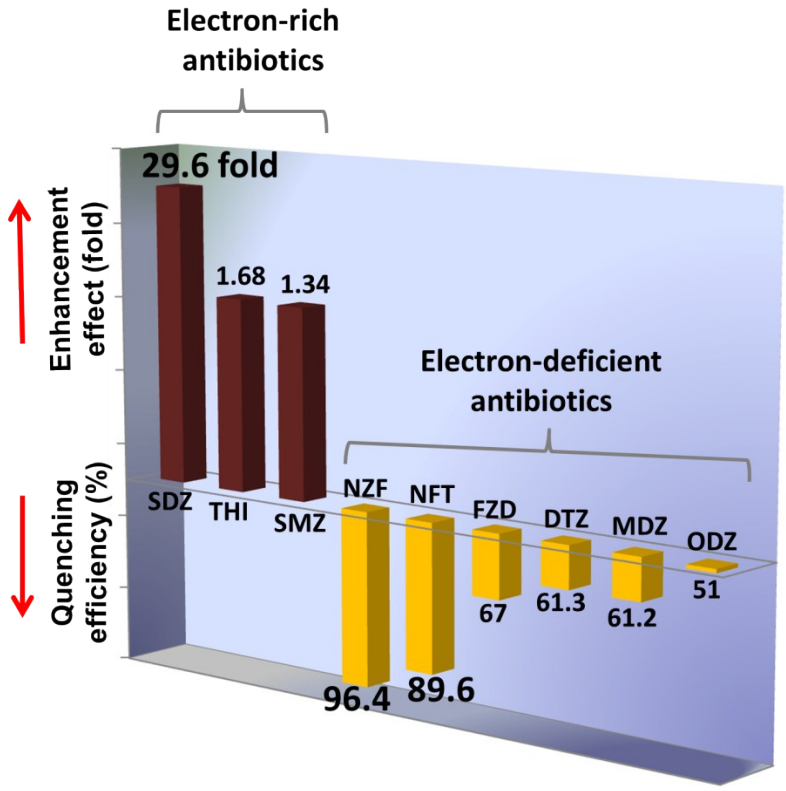

Figure S7. A comparative plot that shows overall peformance of **2a** towards studied electron-rich and electron-deficient antibiotics. Fluorescence quenching efficiency of **2a** (1 mg/ 2 mL DMF) for different antibiotics. Quenching efficiency of **2a** is calculated using equation $(F_0 - F)/F_0 \times 100\%$, where F and F_0 denotes the emission intensities after and before the addition of studied analytes, respectively.

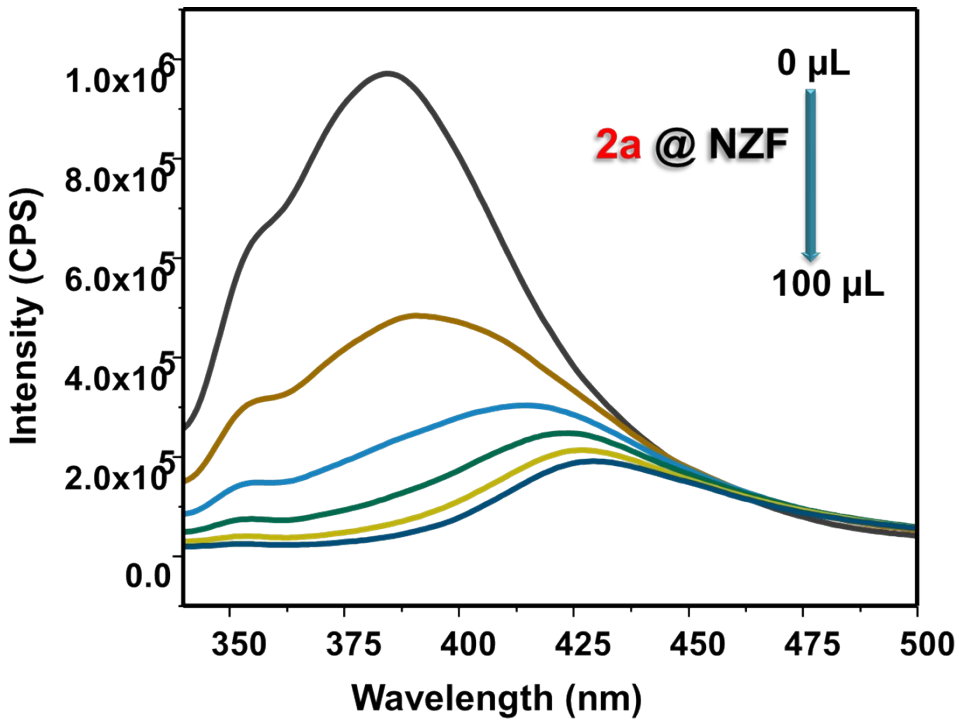

Figure S8. Emission spectra of **2a** upon incremental addition of nitrofurazone (NZF) solution (1 mM).

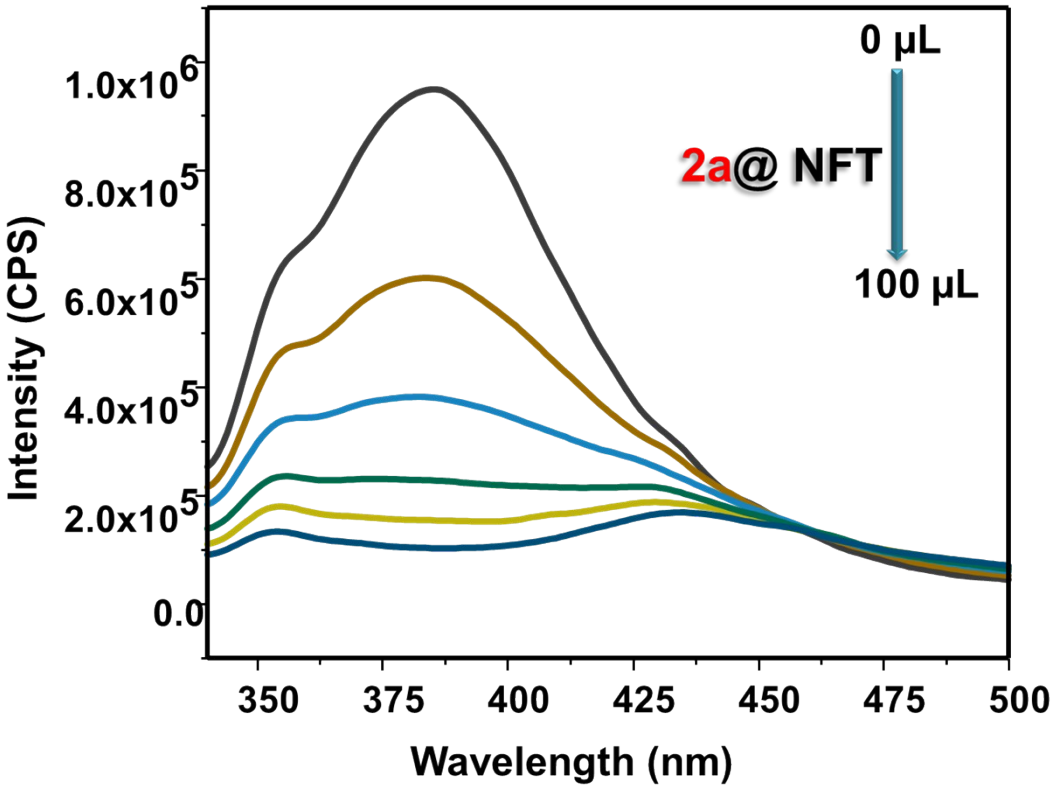

Figure S9. Emission spectra of **2a** upon incremental addition of nitrofurantoin (NFT) solution (1 mM).

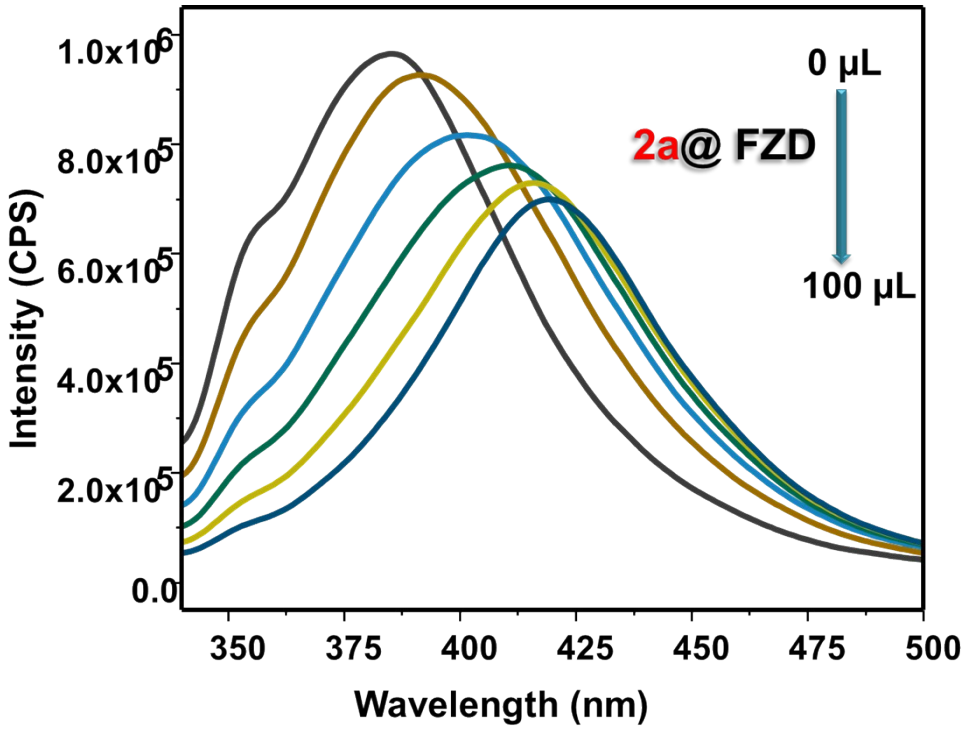

Figure S10. Emission spectra of **2a** upon incremental addition of furazolidone (FZD) solution (1 mM).

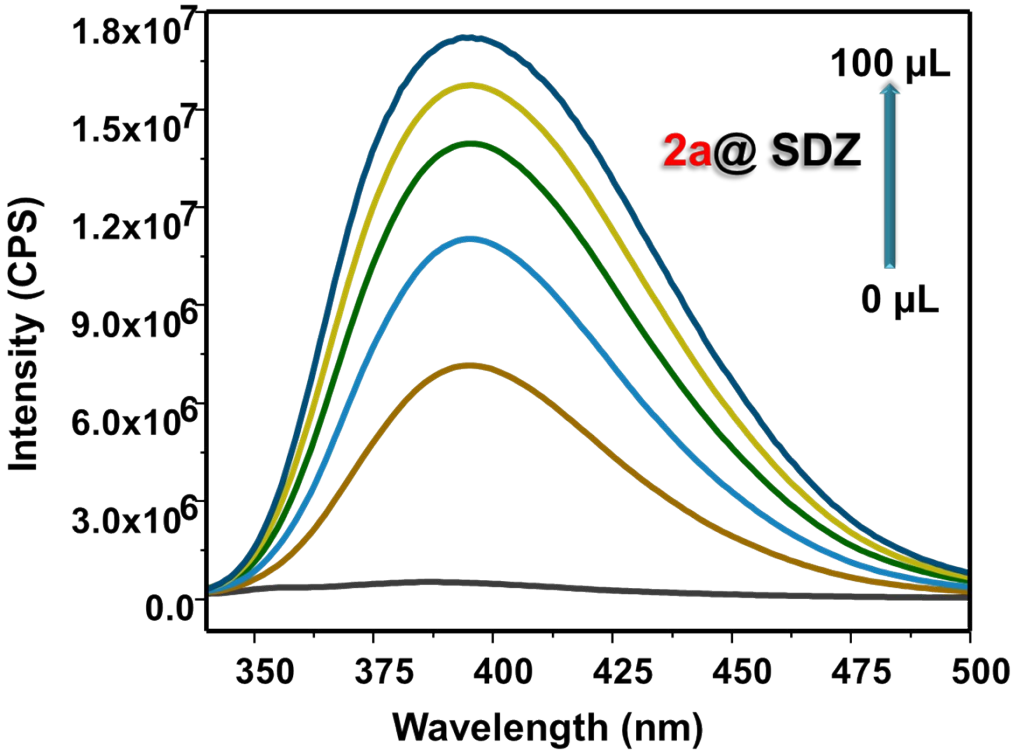

Figure S11. Emission spectra of **2a** upon incremental addition of sulfadiazine (SDZ) solution (1 mM).

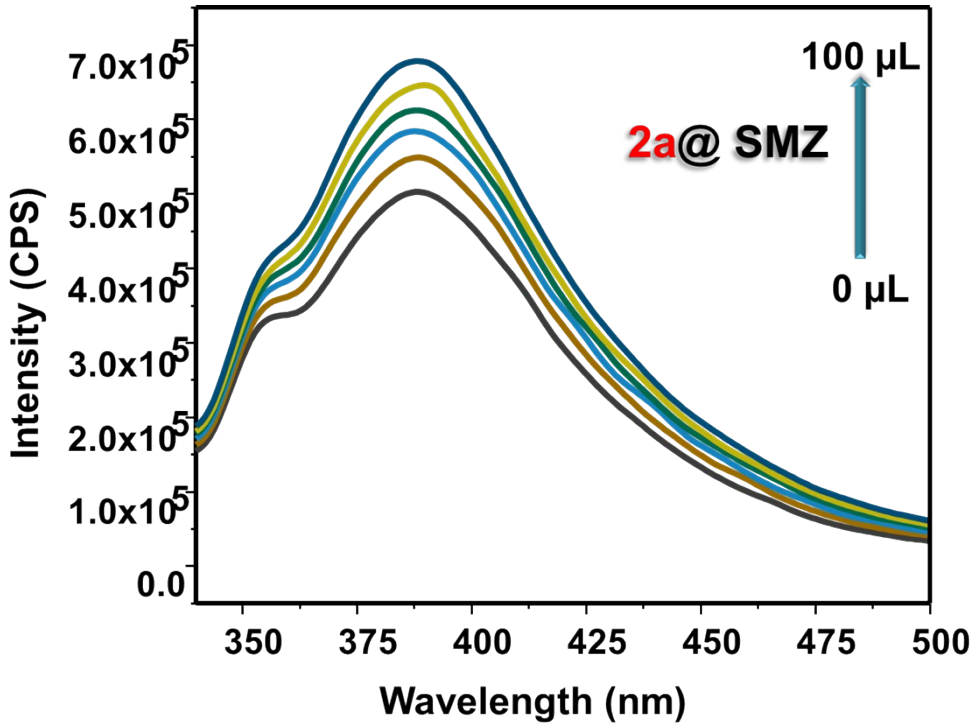

Figure S12. Emission spectra of **2a** upon incremental addition of sulfamethazine (SMZ) solution (1 mM).

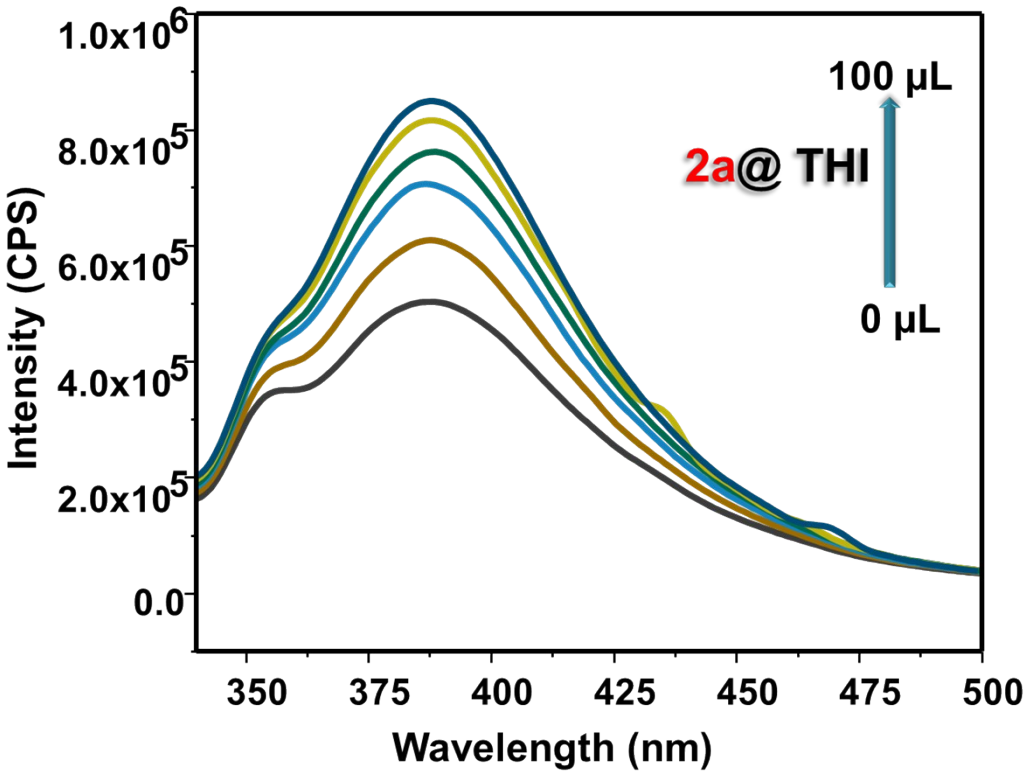

Figure S13. Emission spectra of **2a** upon incremental addition of thiamphenicol (THI) solution (1 mM).

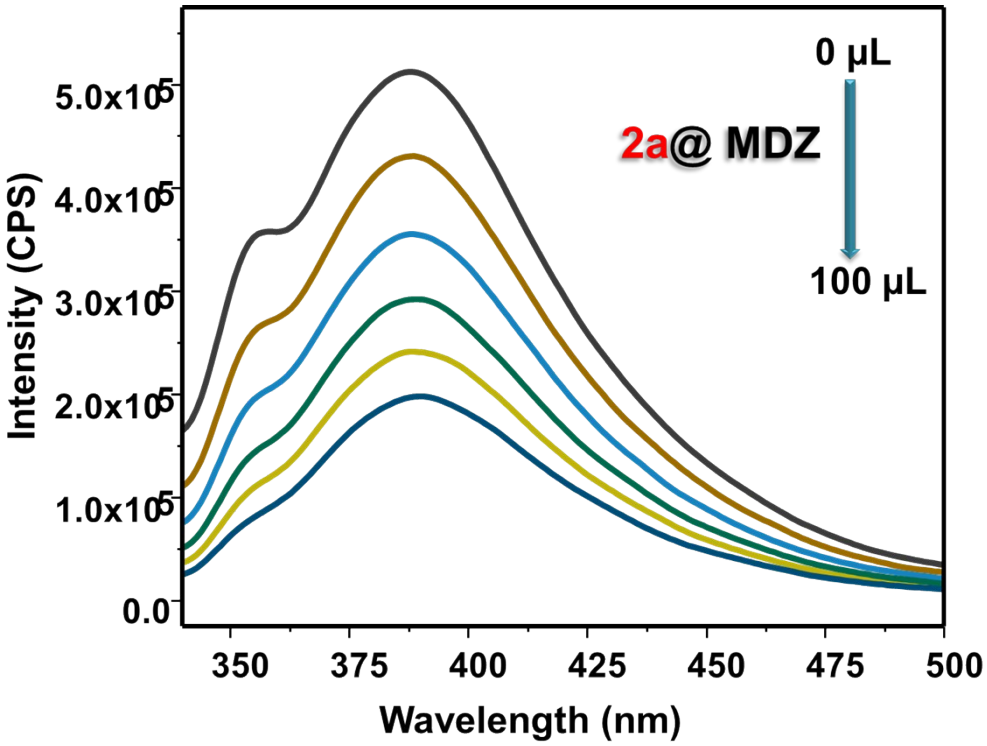

Figure S14. Emission spectra of **2a** upon incremental addition of metronidazole (MDZ) solution (1 mM).

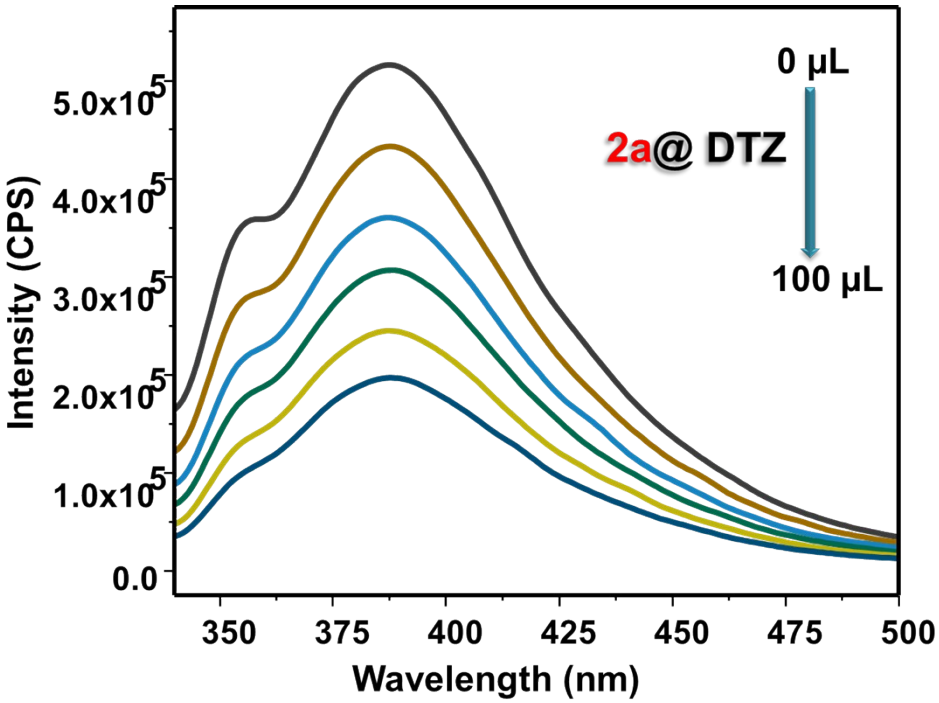

Figure S15. Emission spectra of **2a** upon incremental addition of dimetridazole (DTZ) solution (1 mM).

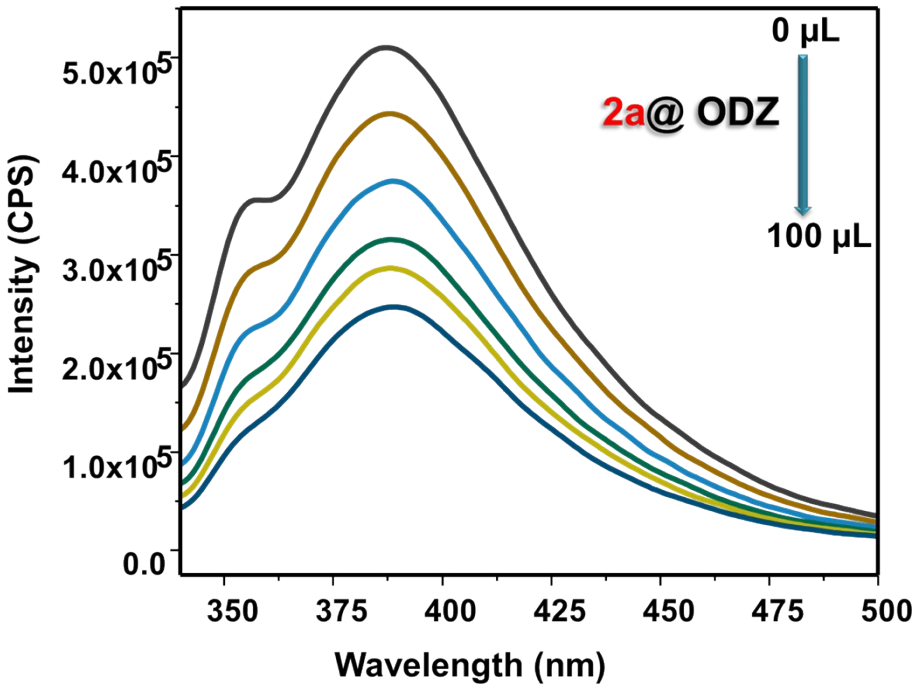

Figure S16. Emission spectra of **2a** upon incremental addition of ornidazole (ODZ) solution (1 mM).

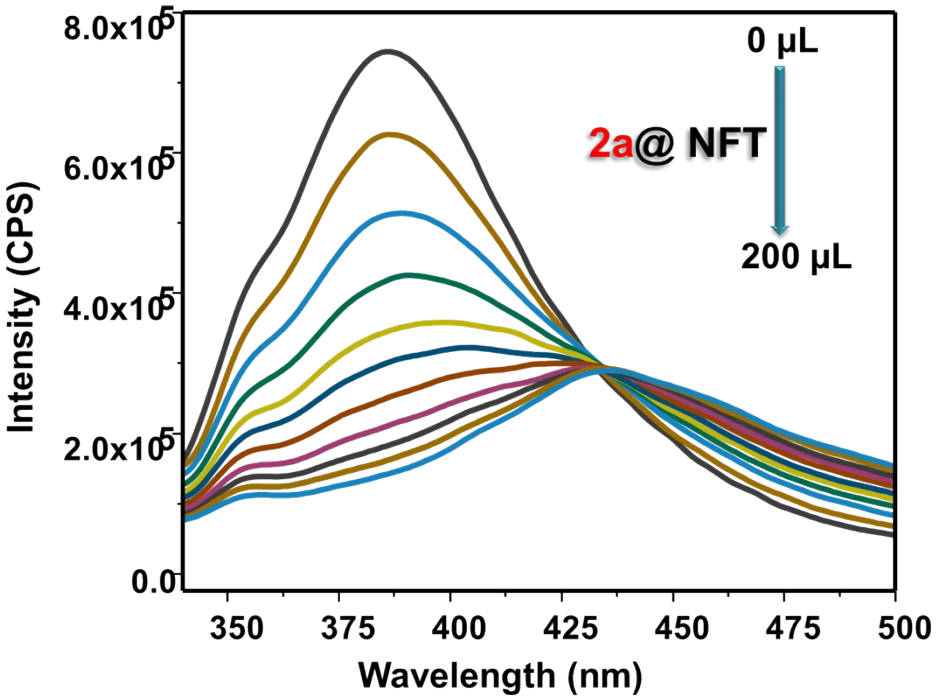

Figure S17. Emission spectra of **2a** upon incremental addition of nitrofurantoin (NFT) solution (1 mM, 200 µL).

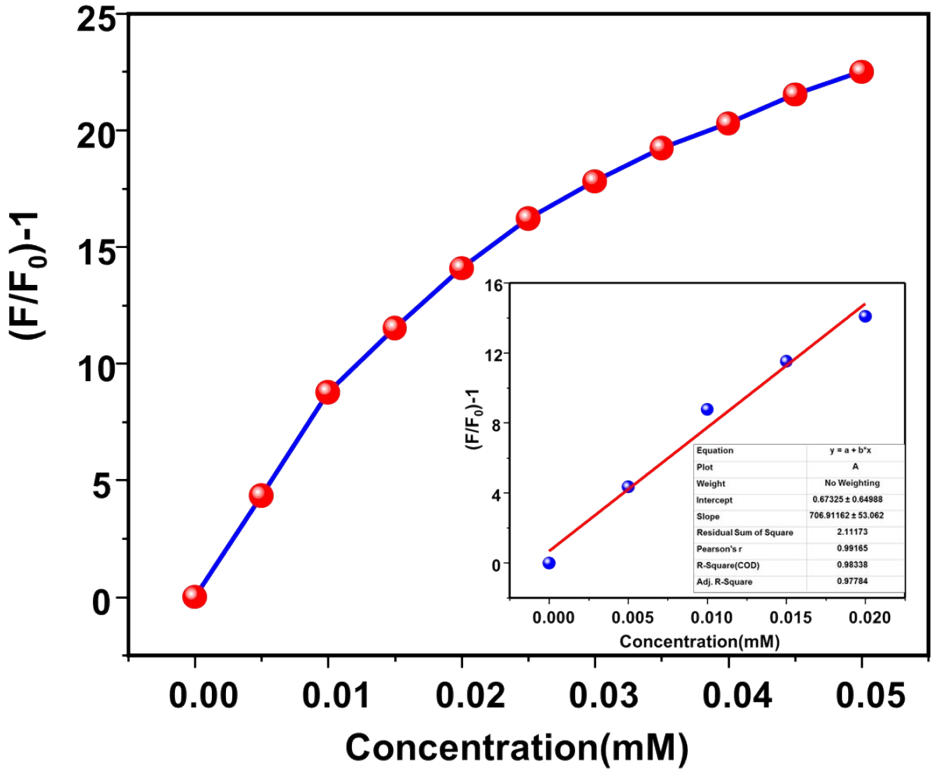

Figure S18. The upward curvature of the plot for SDZ (0–0.05 mM). Inset shows the linear portion of the plot at concentration range 0–0.02 mM.

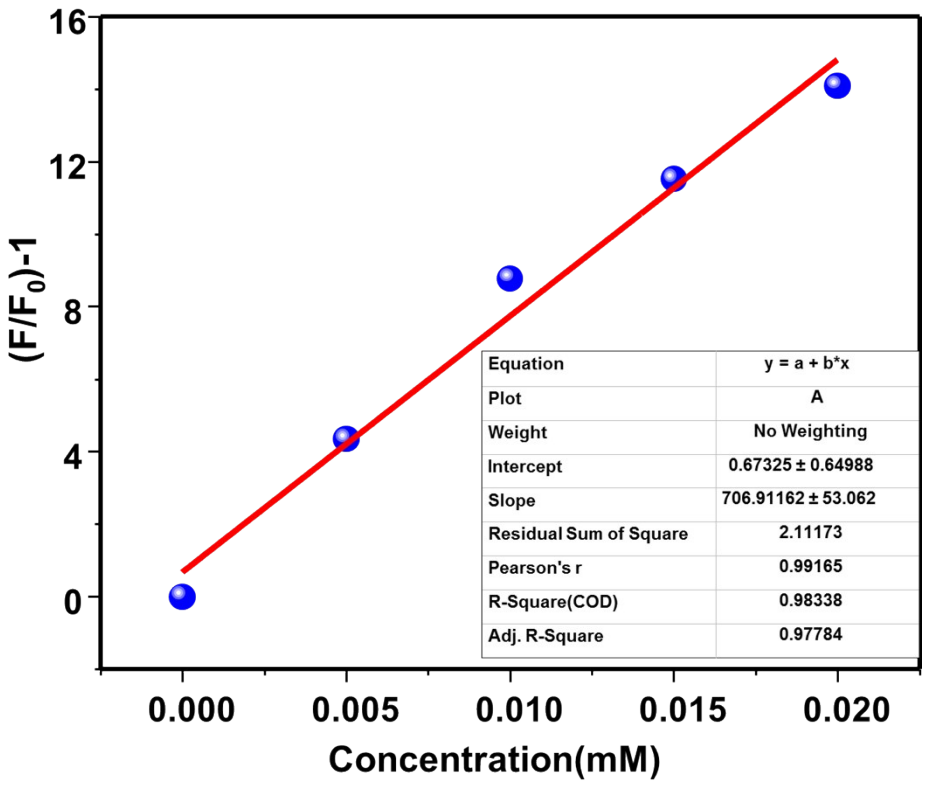

Figure S19. Fluorescence enhancement coefficient (EC) determination plot of **2a**. The relative fluorescence intensity (F/F_0)-1 is linear with SDZ concentration in the range of 0–0.02 mM.

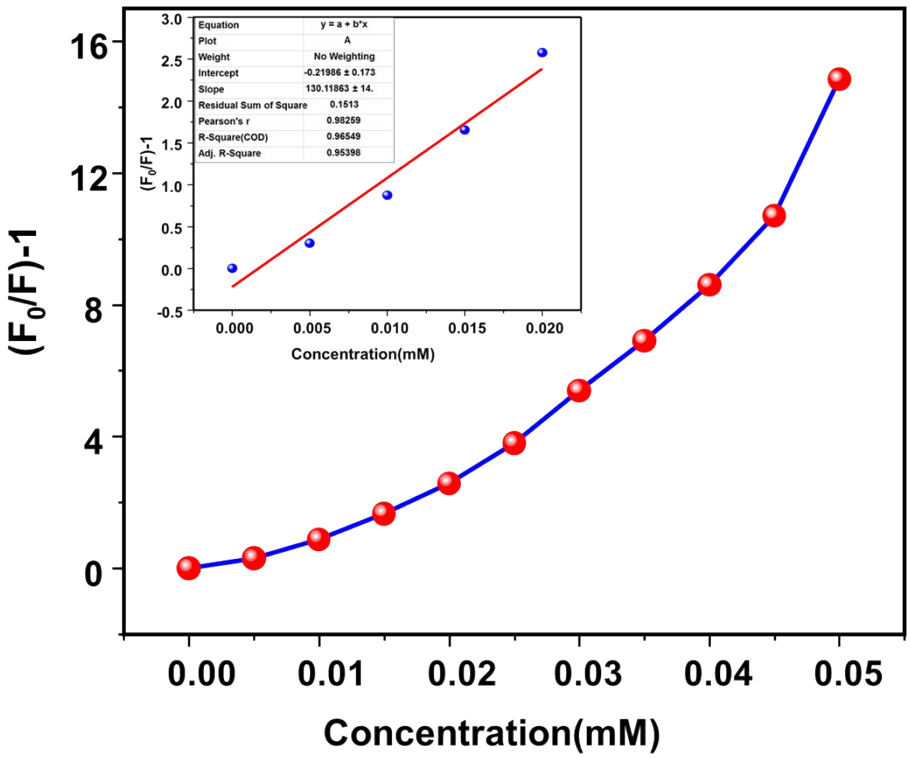

Figure S20. The curvature of the S–V plot for 0.5 mM NZF solution (total concentration 0–0.05 mM). Inset shows the linear portion of the S–V plot at concentration range 0–0.02 mM.

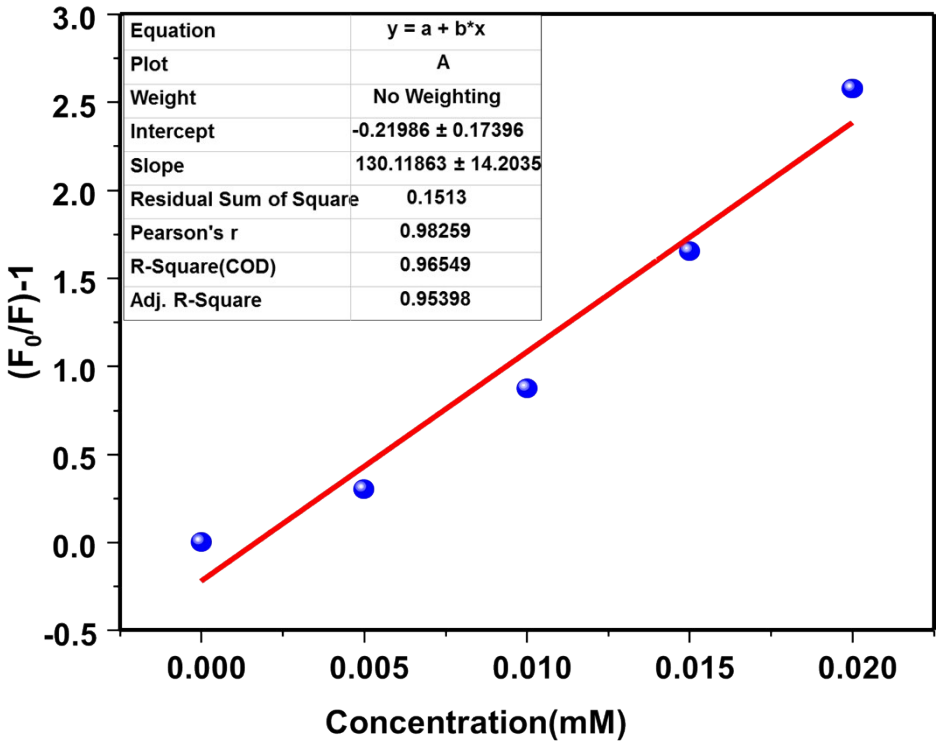

Figure S21. Stern-Volmer (SV) plot for 0.5 mM NZF solution of **2a**. The relative fluorescence intensity $(F_0/F)-1$ is linear with NZF concentration in the range of 0–0.02 mM.

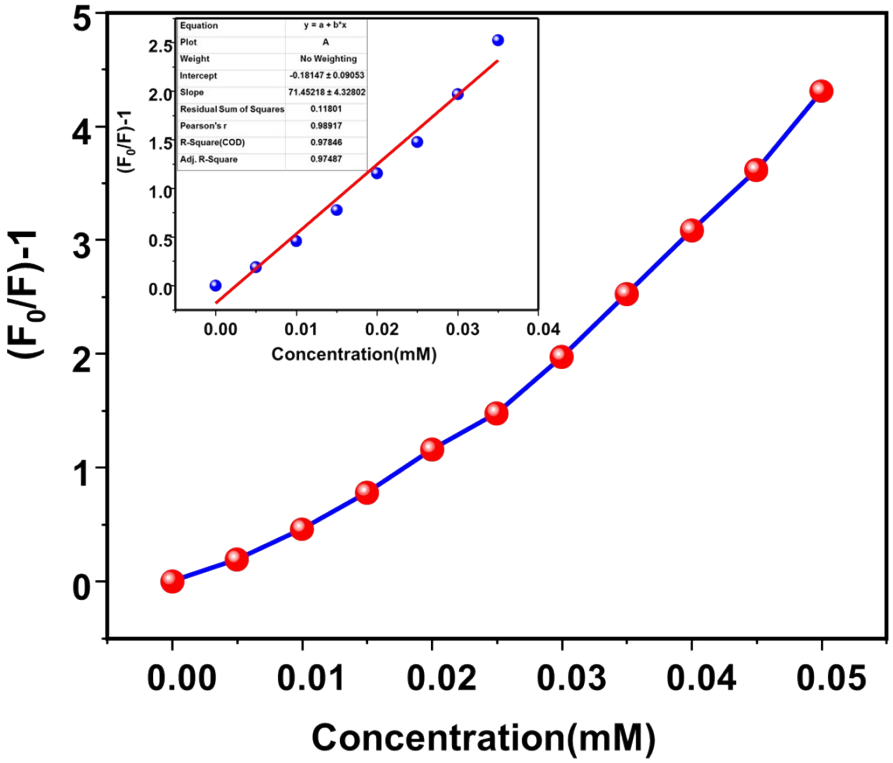

Figure S22. The curvature of the S–V plot for 0.5 mM NFT solution (total concentration 0–0.05 mM). Inset shows the linear portion of the S–V plot at concentration range 0–0.035 mM.

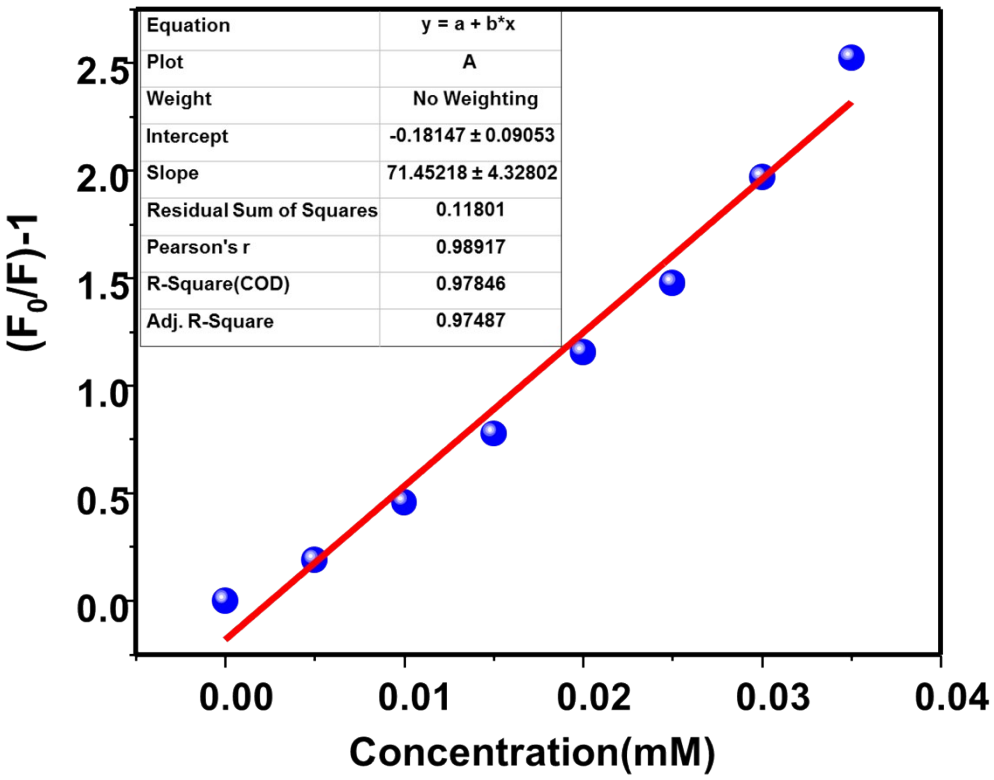

Figure S23. Stern-Volmer (SV) plot for 0.5 mM NFT solution of **2a**. The relative fluorescence intensity $(F_0/F)-1$ is linear with NFT concentration in the range of 0–0.035 mM.

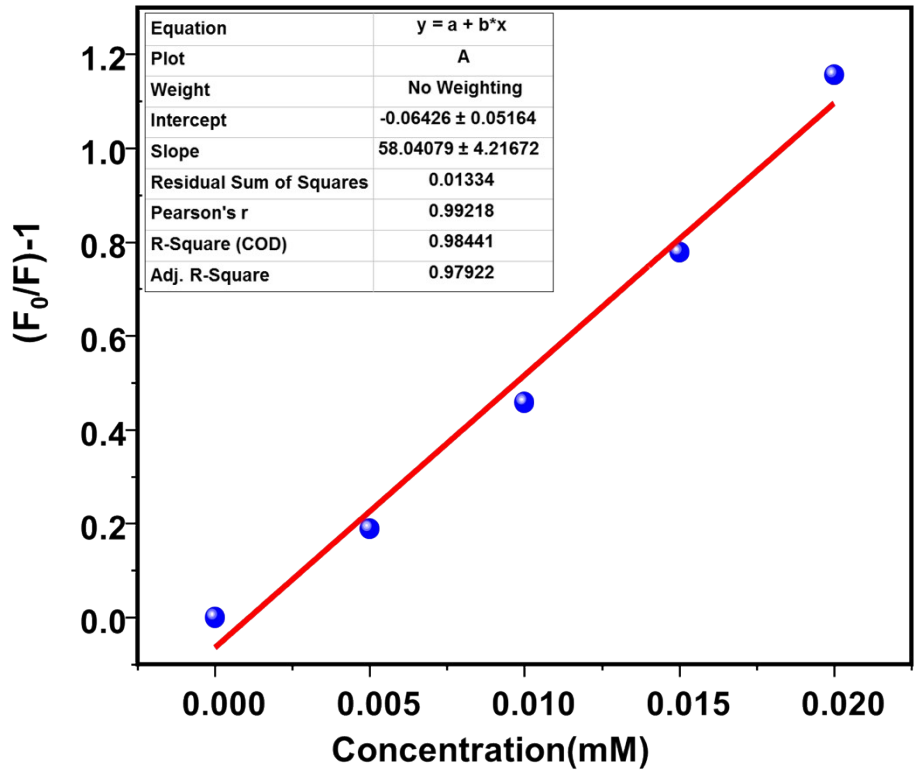

Figure S24. Stern-Volmer (SV) plot for 1 mM FZD solution of **2a**. The relative fluorescence intensity $(F_0/F)-1$ is linear with FZD concentration in the range of 0–0.02 mM.

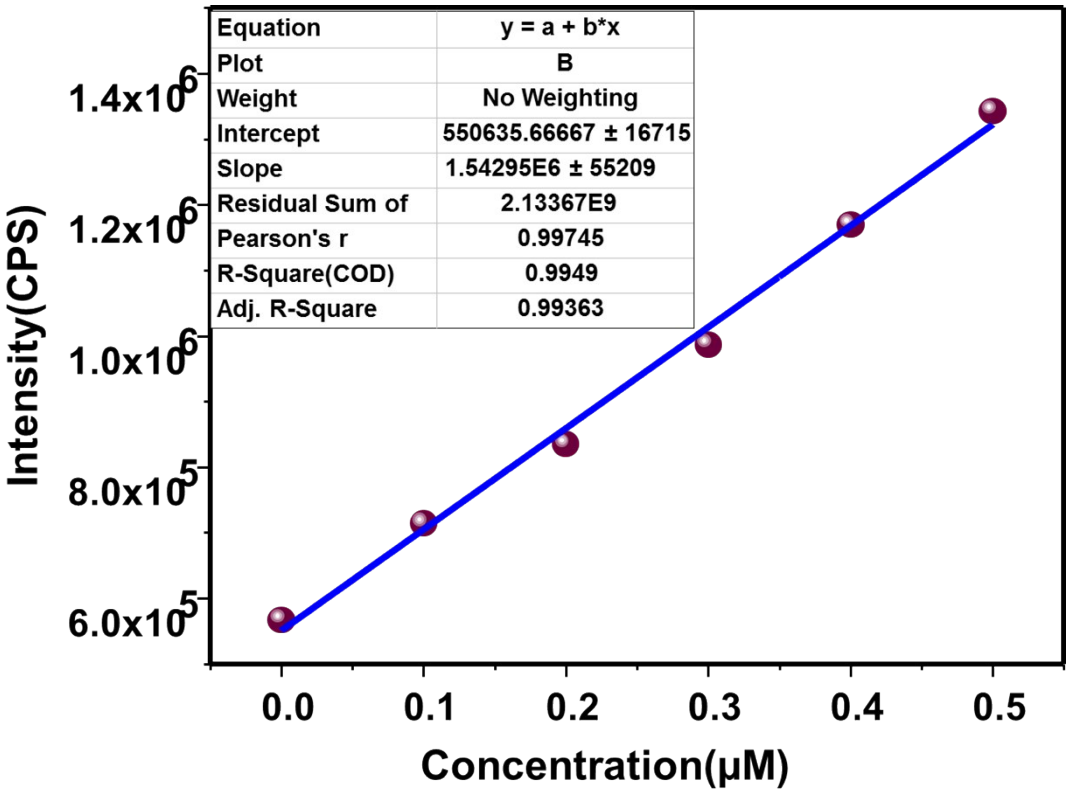

Figure S25. Linear region of fluorescence intensity of **2a** upon addition of SDZ (0 – 100 μL, 10 μM stock solution).

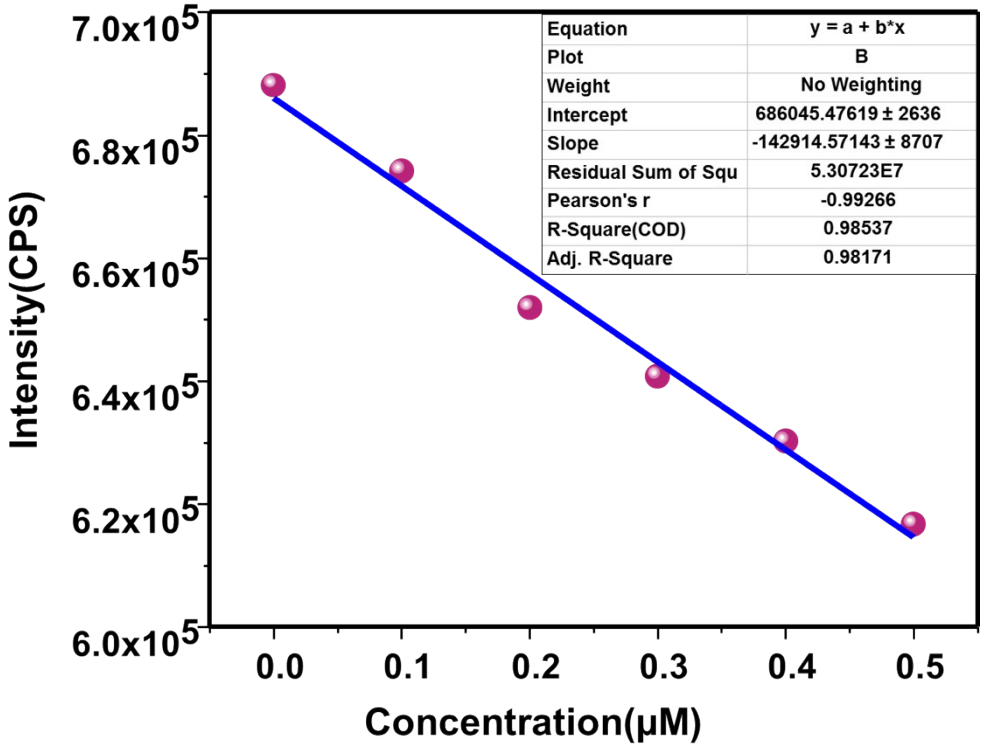

Figure S26. Linear region of fluorescence intensity of **2a** upon addition of NZF (0 – 100 μL, 10 μM stock solution).

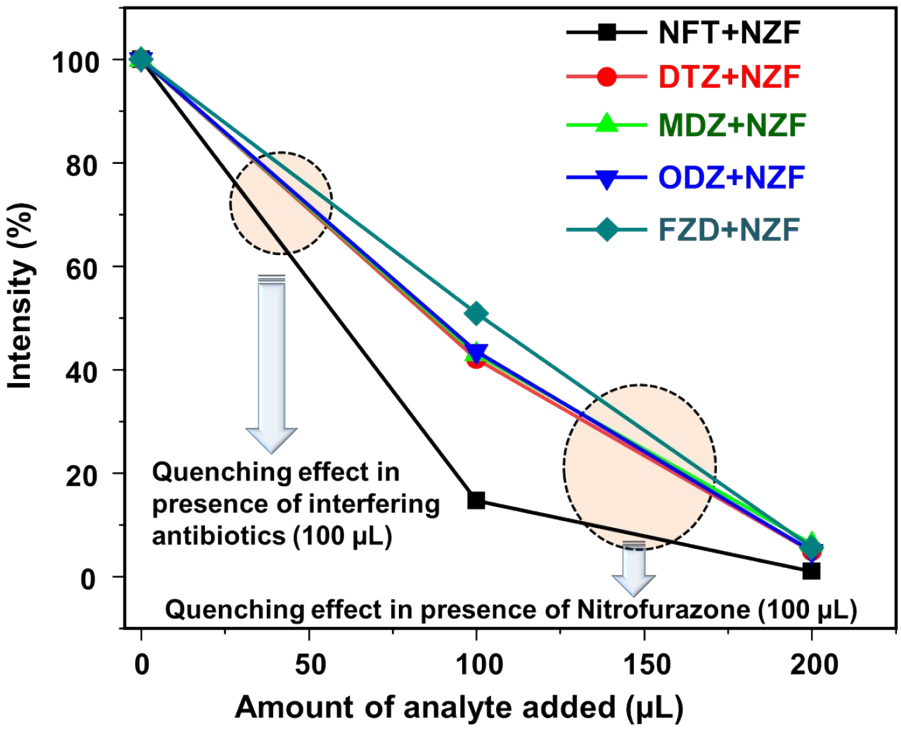

Figure S27. The plot of interference test, showing decrease in fluorescence intensities upon addition of different electron deficient antibiotics (1 mM, 100 µL), followed by NZF (1 mM, 100 µL) to **2a**.

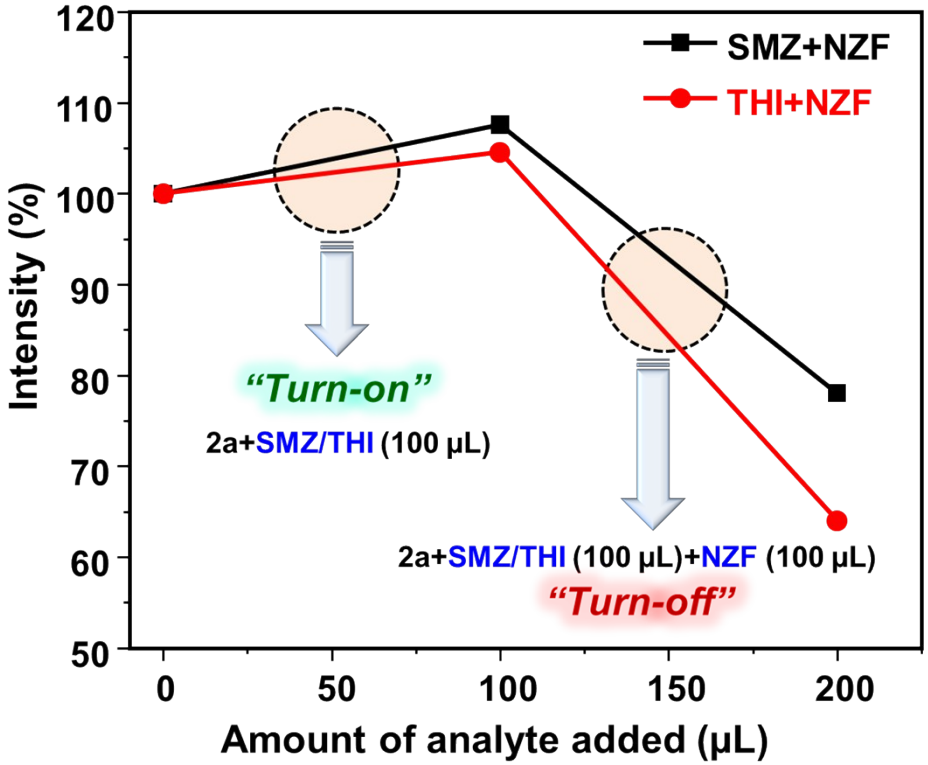

Figure S28. The plot of interference test, showing increase in fluorescence intensities upon addition of different electron rich antibiotics (SMZ/THI) (1 mM, 100 µL), followed by NZF (1 mM, 100 µL) to **2a**.

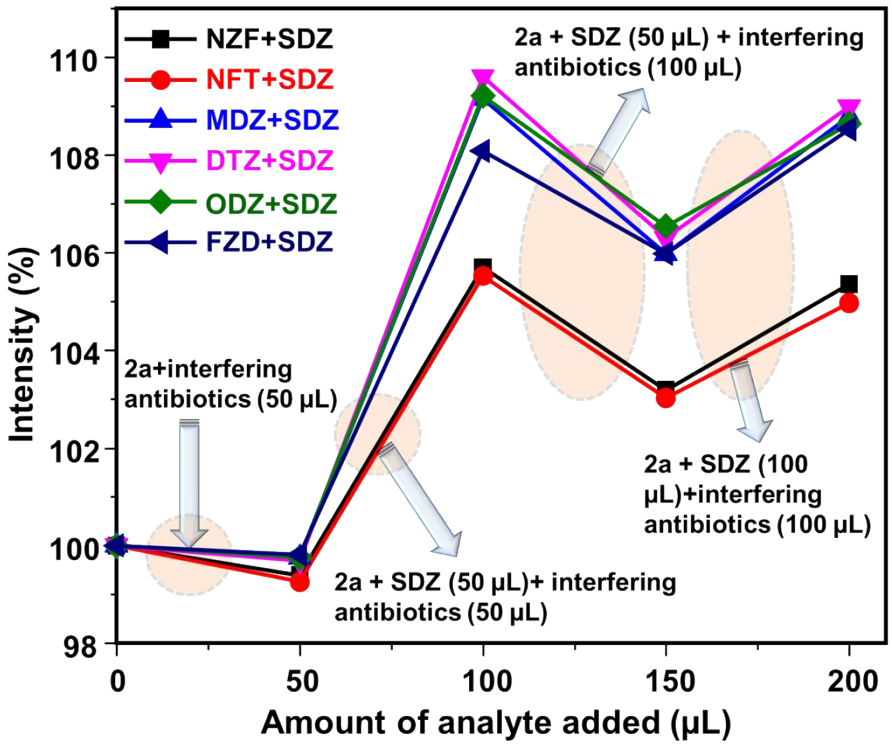

Figure S29. Interference plot showing selective turn-on response for SDZ in presence of other electron deficient antibiotics shows turn-off response.

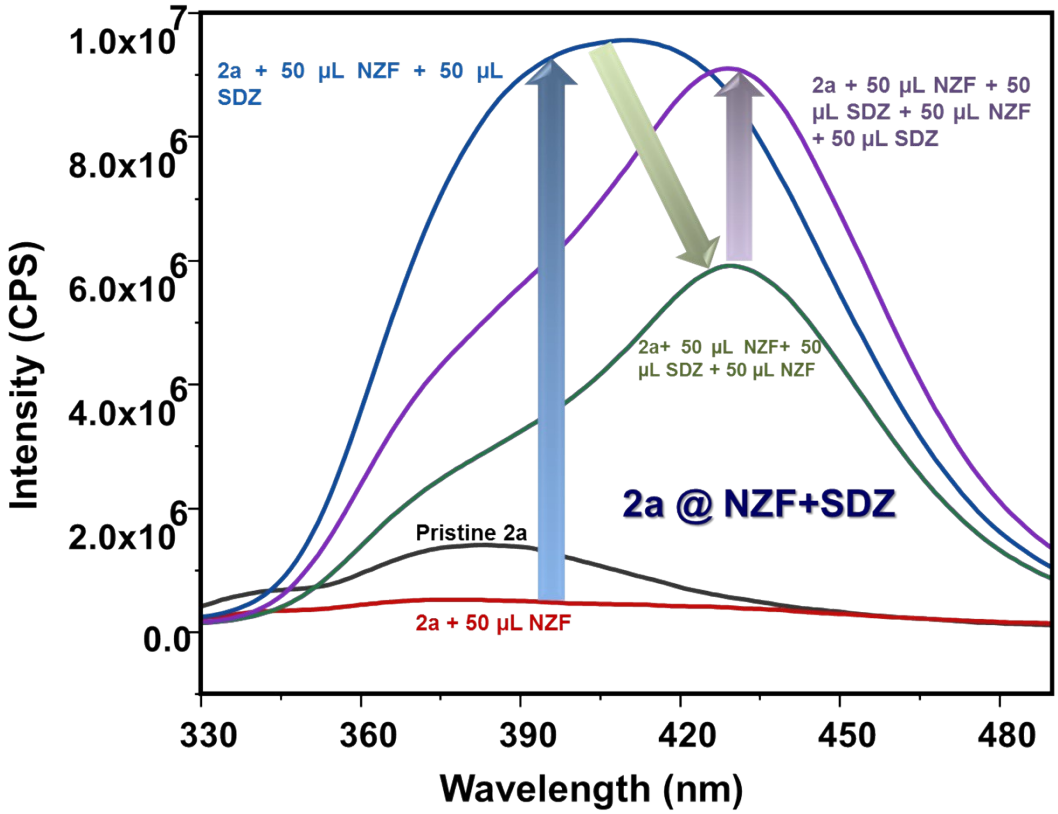

Figure S30. Change in fluorescence spectrum of **2a**, upon simultaneous addition of SDZ in presence of NZF (0 µL -200 µL, 50 µL alternating addition of each analyte).

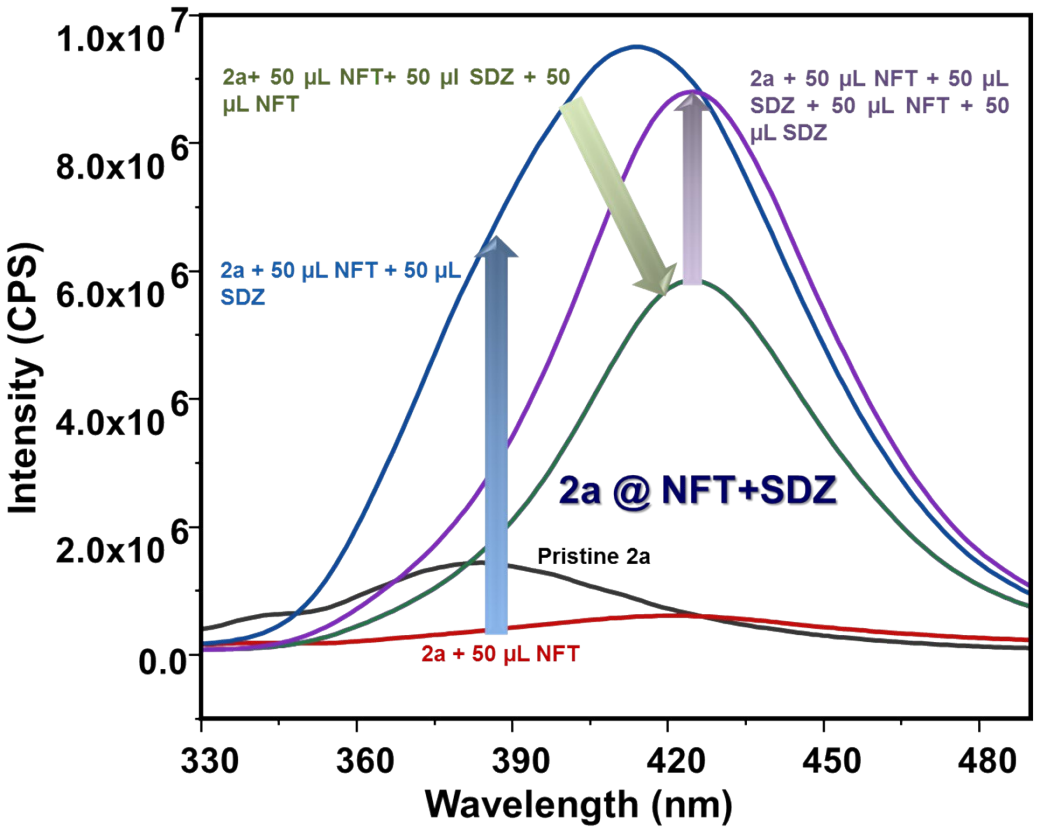

Figure S31. Change in fluorescence spectrum of **2a**, upon simultaneous addition of SDZ in presence of NFT (0 µL -200 µL, 50 µL alternating addition of each analyte).

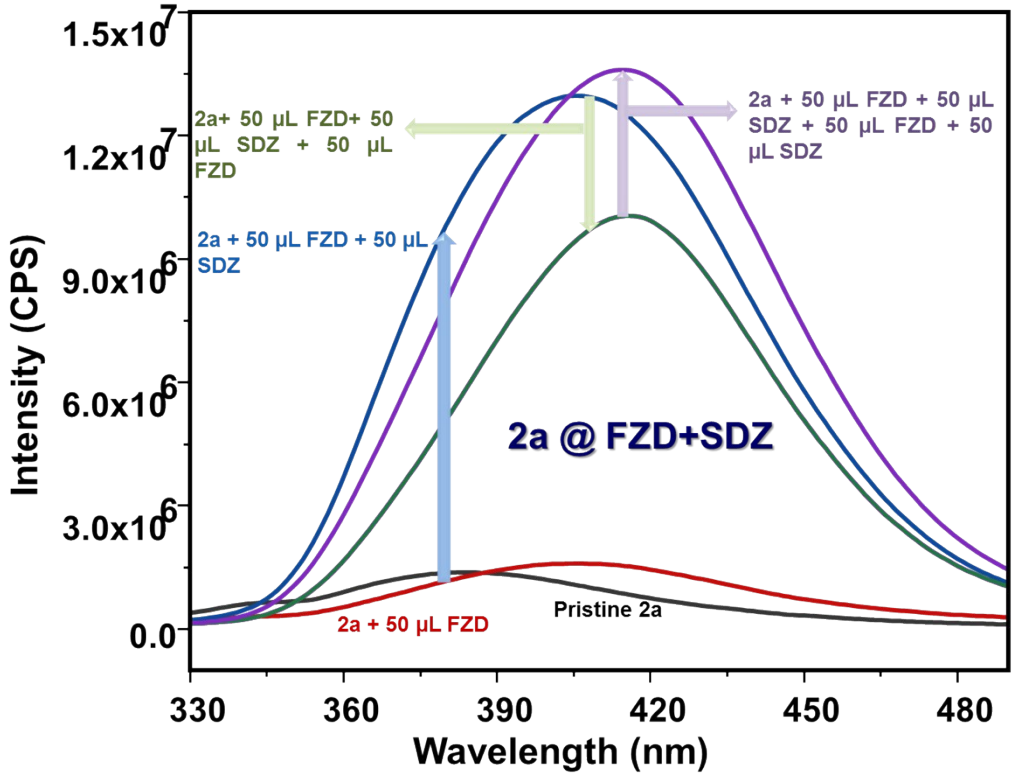

Figure S32. Change in fluorescence spectrum of **2a**, upon simultaneous addition of SDZ in presence of FZD (0 µL -200 µL, 50 µL alternating addition of each analyte).

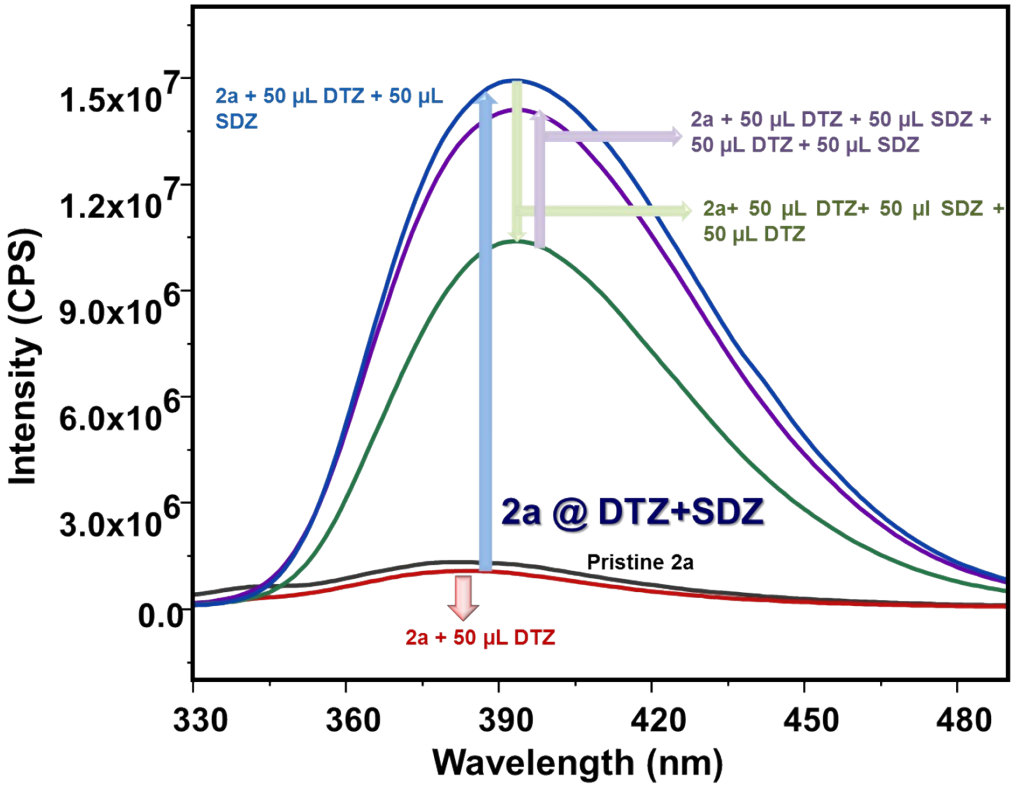

Figure S33. Change in fluorescence spectrum of **2a**, upon simultaneous addition of SDZ in presence of DTZ (0 µL -200 µL, 50 µL alternating addition of each analyte).

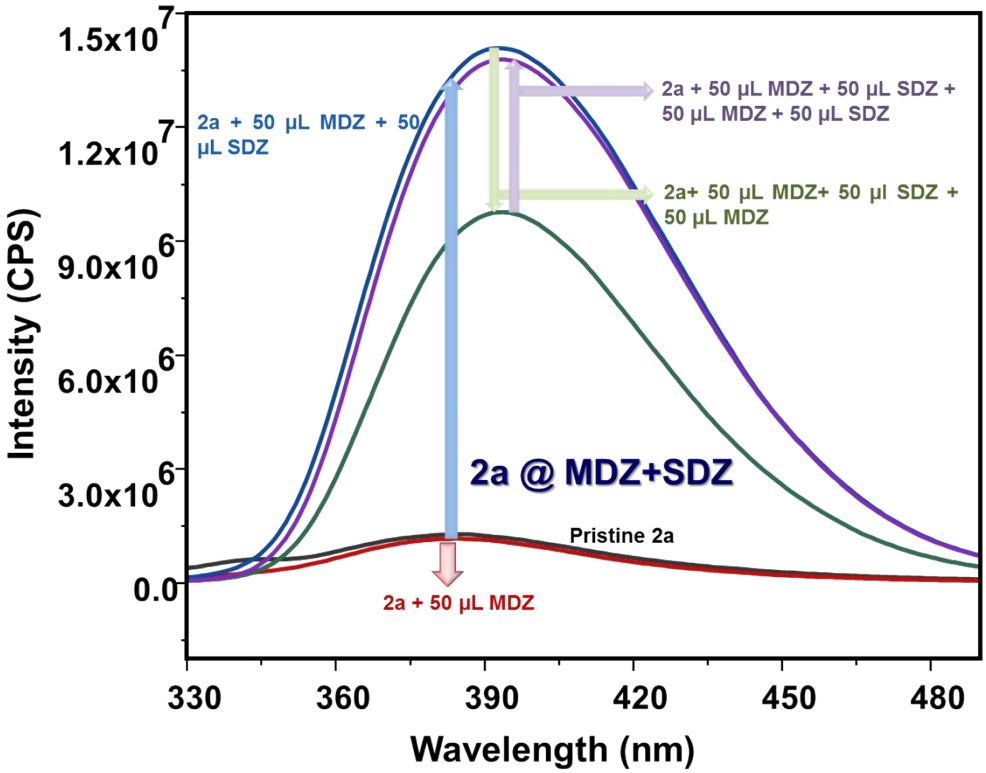

Figure S34. Change in fluorescence spectrum of **2a**, upon simultaneous addition of SDZ in presence of MDZ (0 µL -200 µL, 50 µL alternating addition of each analyte).

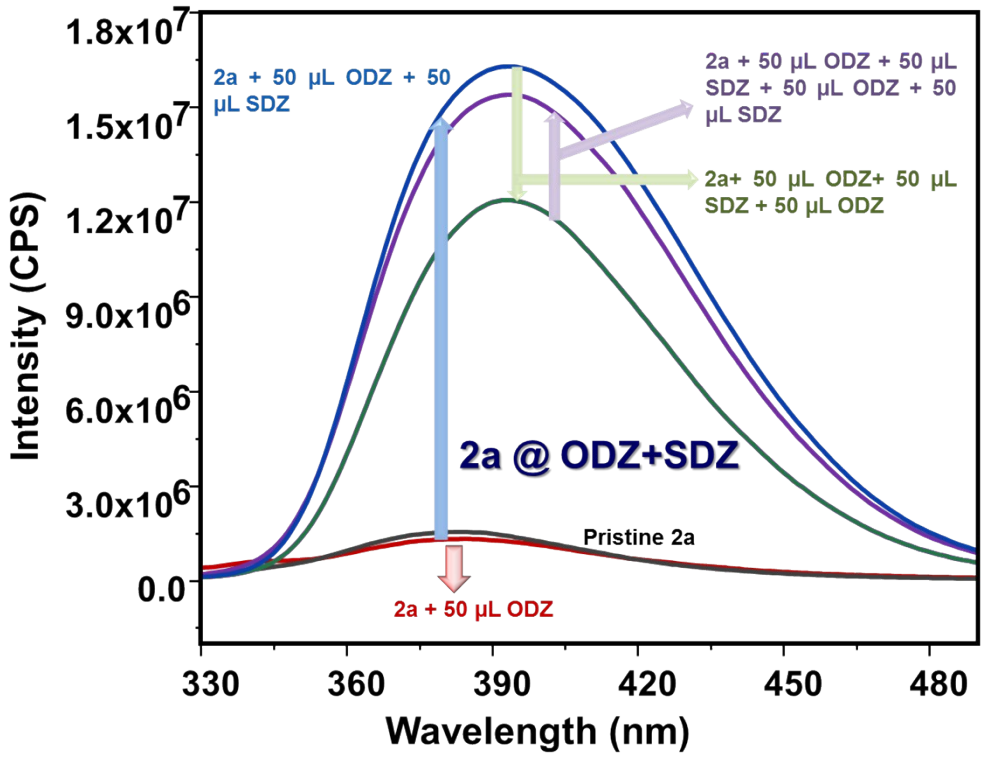

Figure S35. Change in fluorescence spectrum of **2a**, upon simultaneous addition of SDZ in presence of ODZ (0 µL -200 µL, 50 µL alternating addition of each analyte).

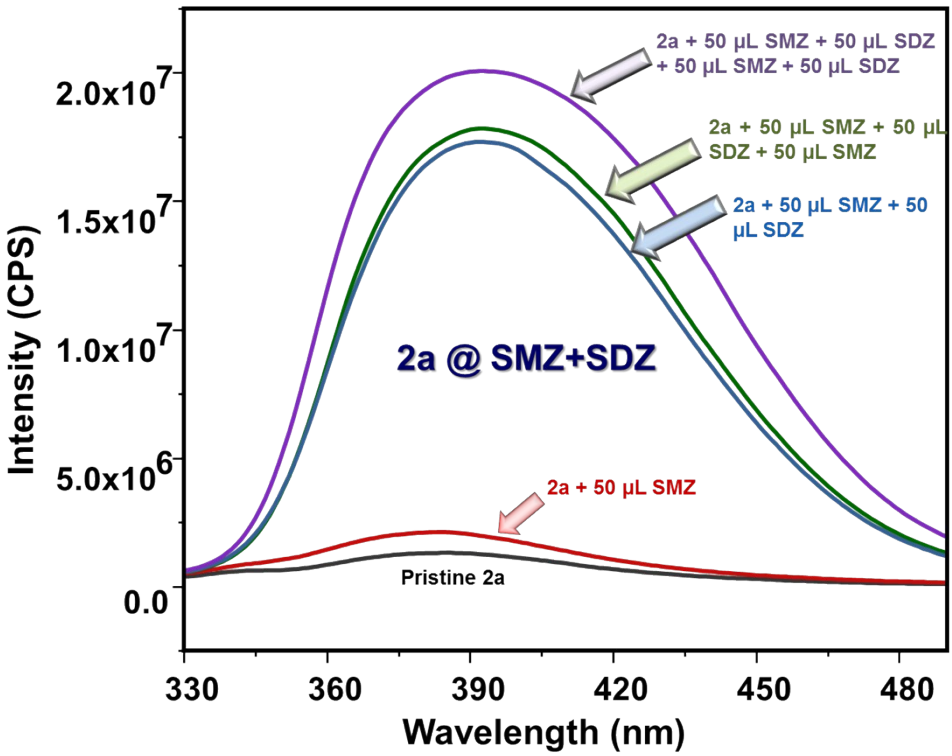

Figure S36. Change in fluorescence spectrum of **2a**, upon simultaneous addition of SDZ in presence of SMZ (0 µL -200 µL, 50 µL alternating addition of each analyte).

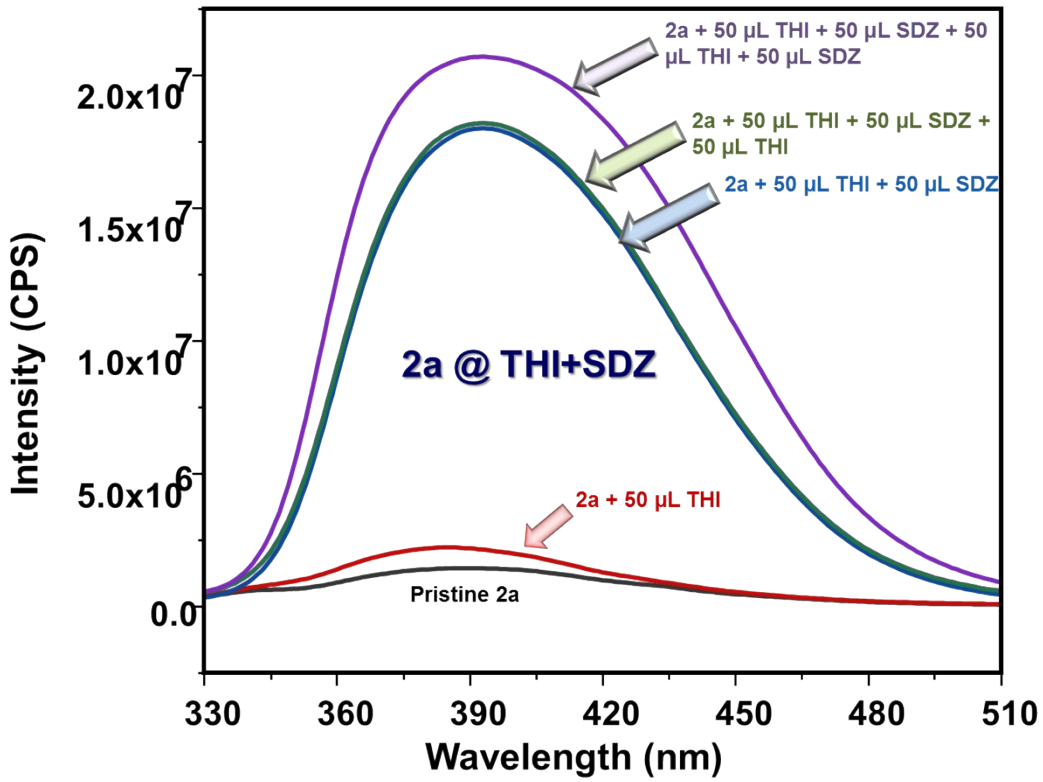

Figure S37. Change in fluorescence spectrum of **2a**, upon simultaneous addition of SDZ in presence of THI (0 µL -200 µL, 50 µL alternating addition of each analyte).

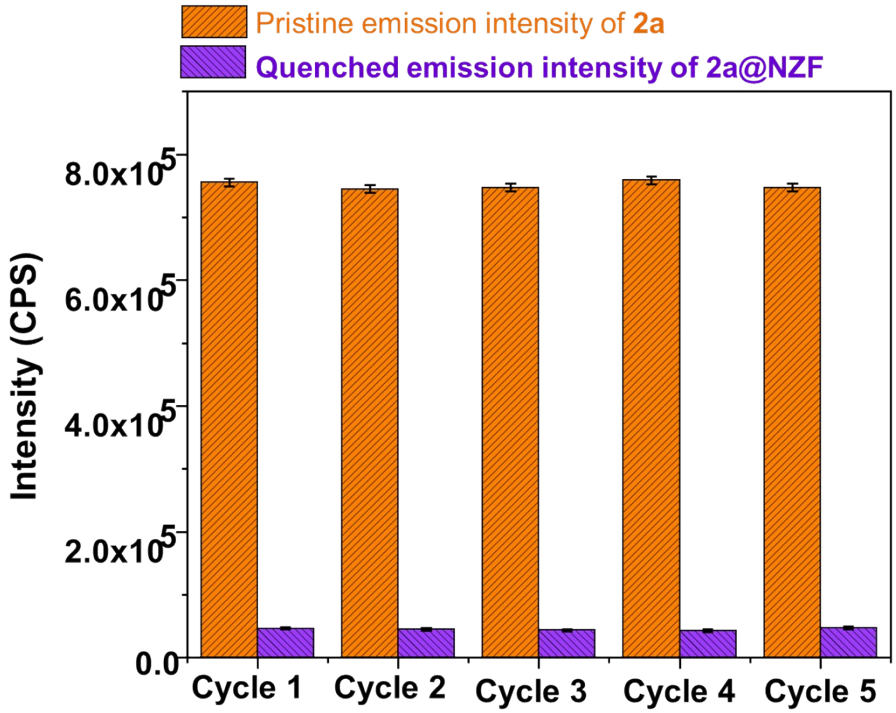

Figure S38. Reproducibility of quenching efficiency of **2a** towards 1 mM NZF solution up to 5 cycles.

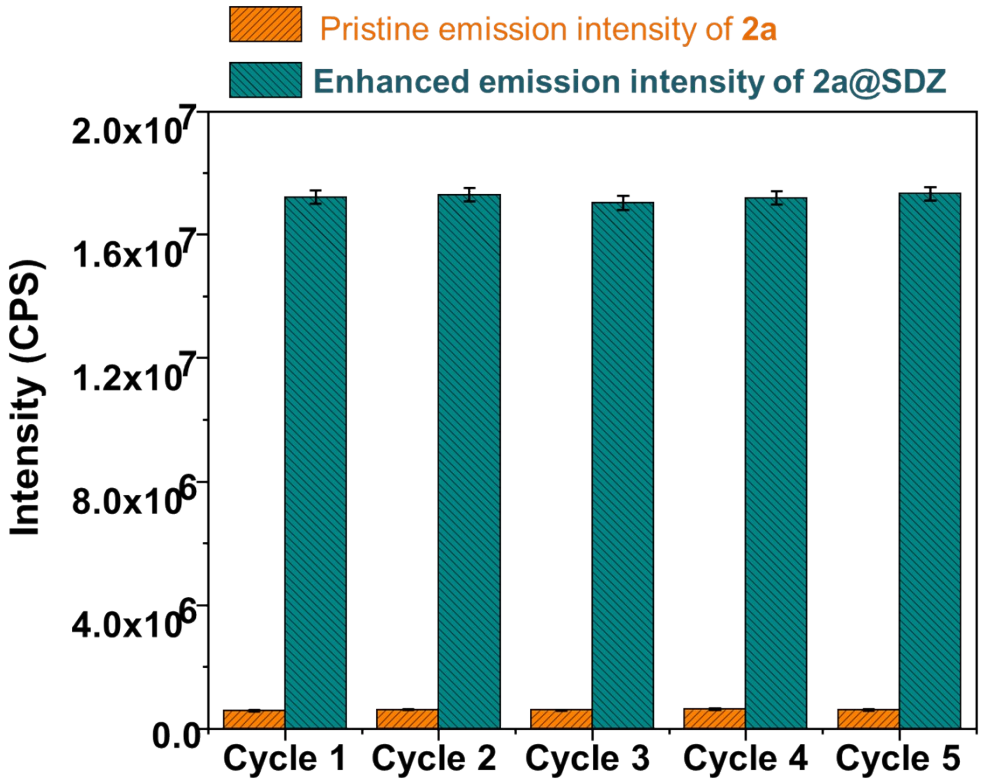

Figure S39. Reproducibility of enhancing efficiency of **2a** towards 1 mM SDZ solution up to 5 cycles.

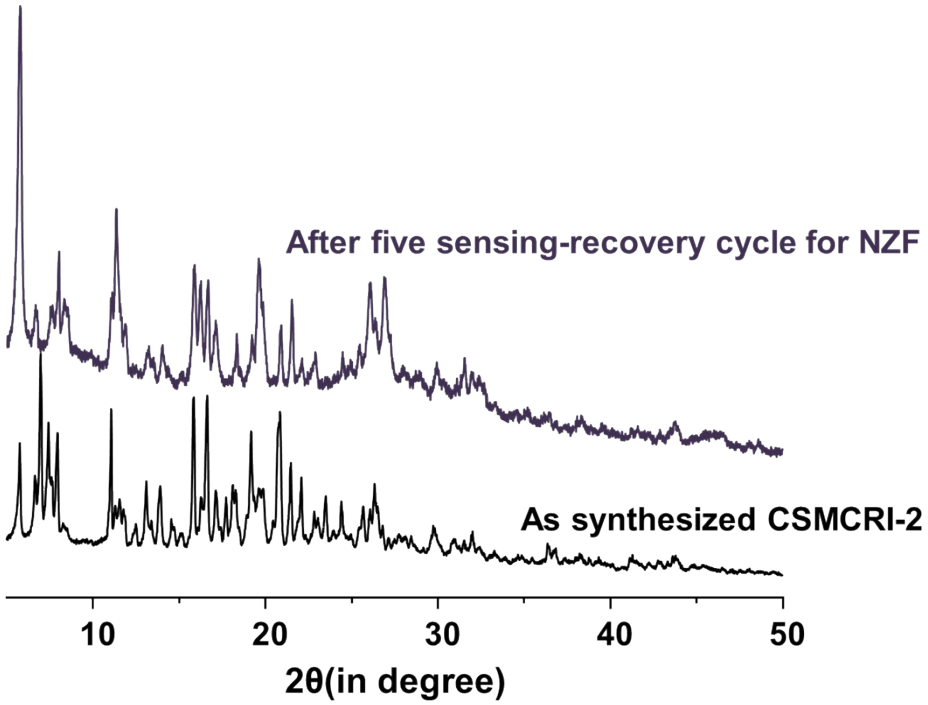

Figure S40. PXRD curves of **2a** after five sensing recovery cycles for NZF (1 mM), showing that structural integrity of the framework is maintained.

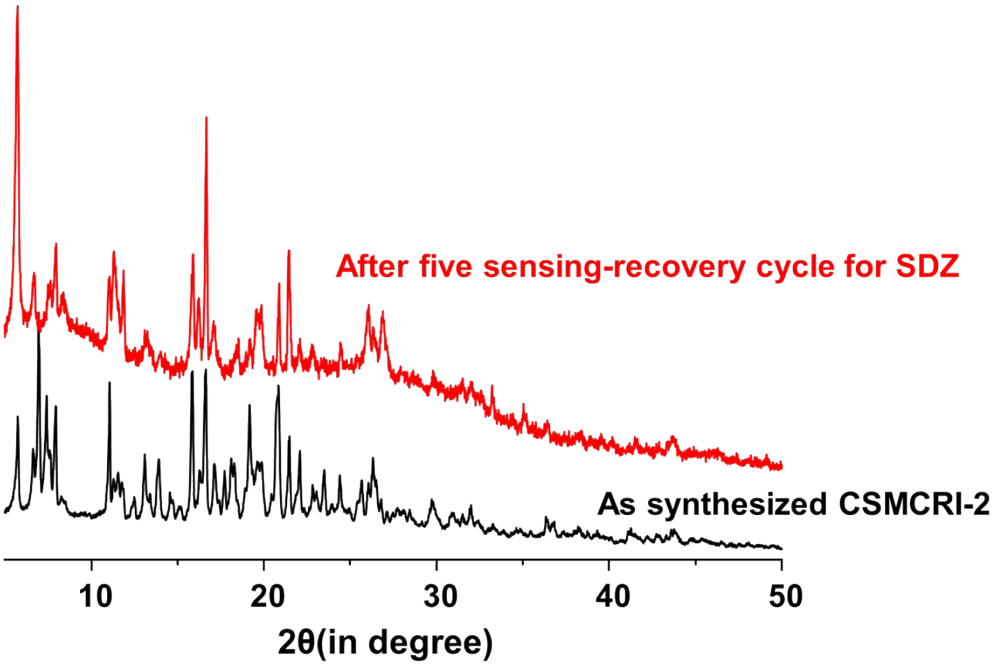

Figure S41. PXRD curves of **2a** after five sensing recovery cycles for SDZ (1 mM), showing that structural integrity of the framework is maintained.

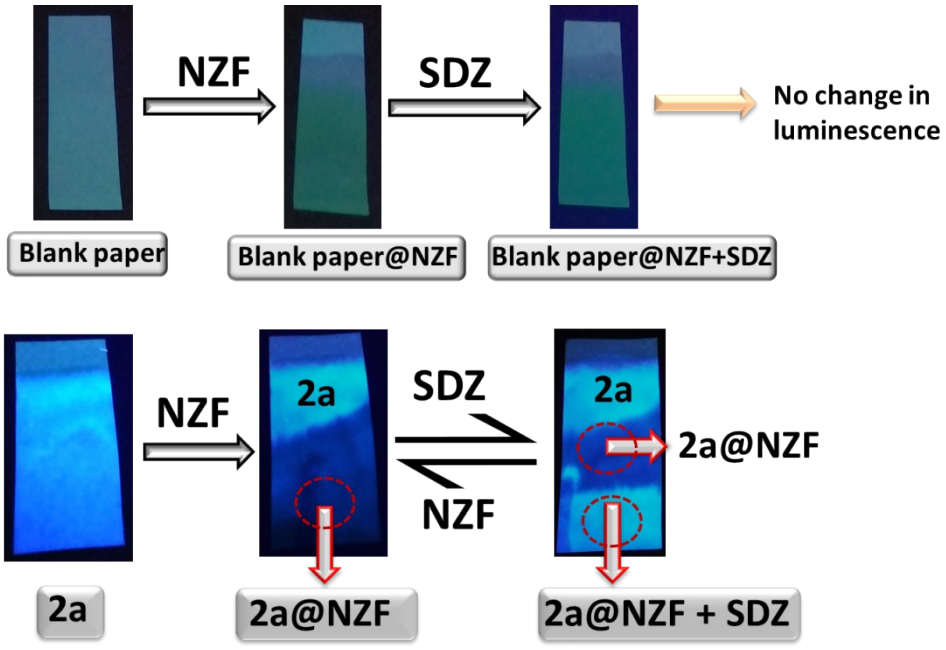

Figure S42. Comparison between Blank paper strip (top) and **2a** coated paper strip (bottom) for naked eye detection of NZF and SDZ under UV light (365 nm) corroborating that **2a** is necessary for fluorescence switching.

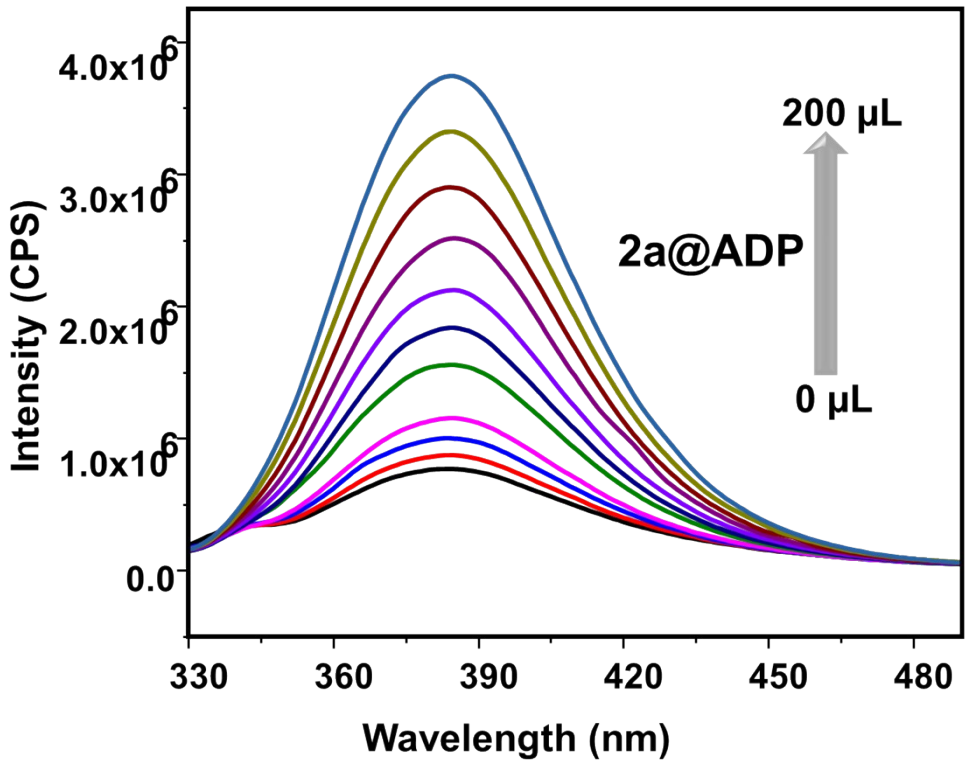

Figure S43. Emission spectra of **2a** upon incremental addition of adenosine diphosphate (ADP) solution (1 mM).

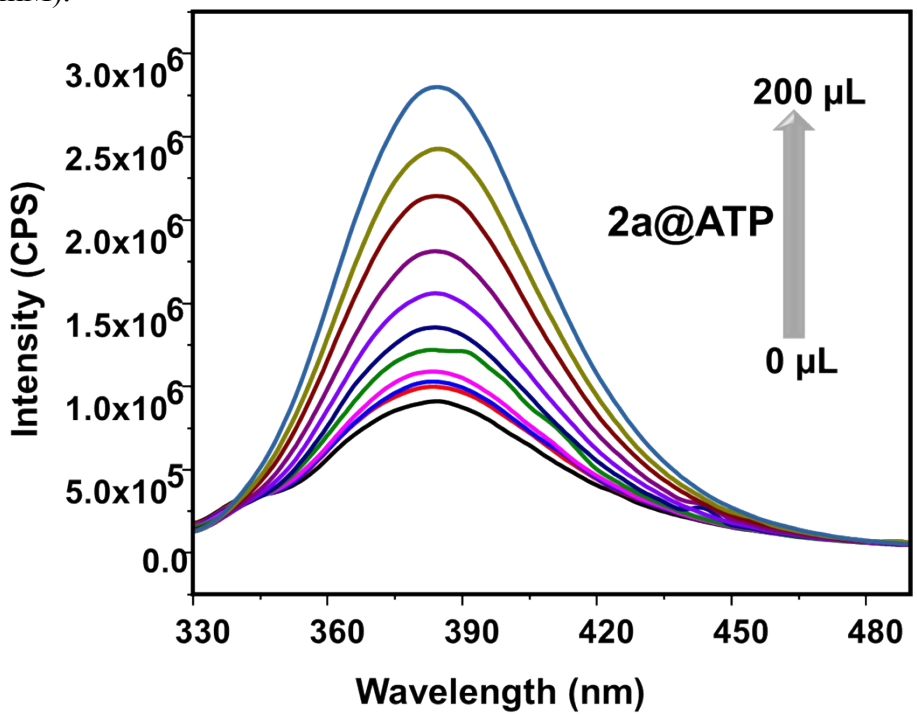

Figure S44. Emission spectra of **2a** upon incremental addition of adenosine triphosphate (ATP) solution (1 mM).

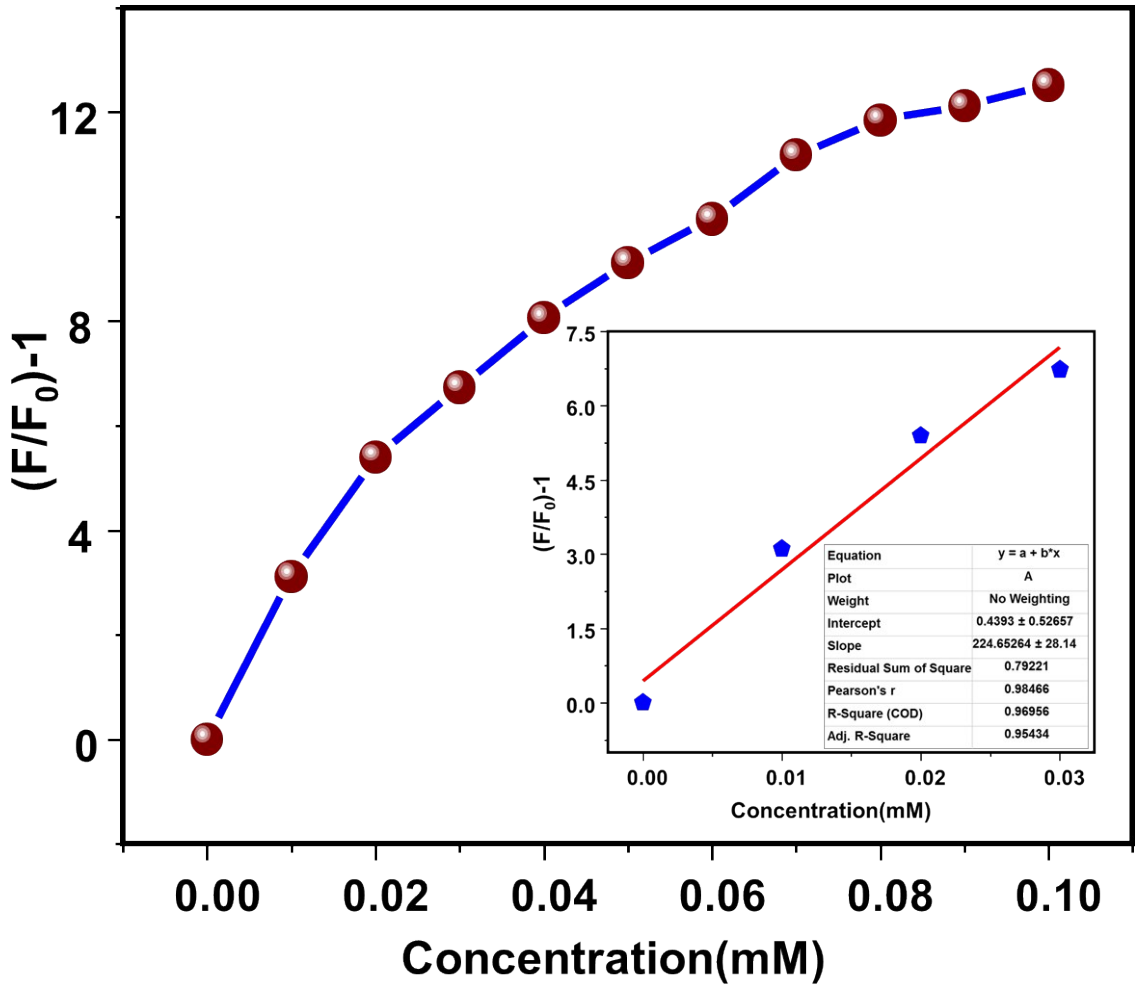

Figure S45. The upward curvature of the plot for 1 mM AMP solution (total concentration 0–0.1 mM, 0 µL -200 µL). Inset shows the linear portion of the S–V plot at concentration range 0–0.03 mM.

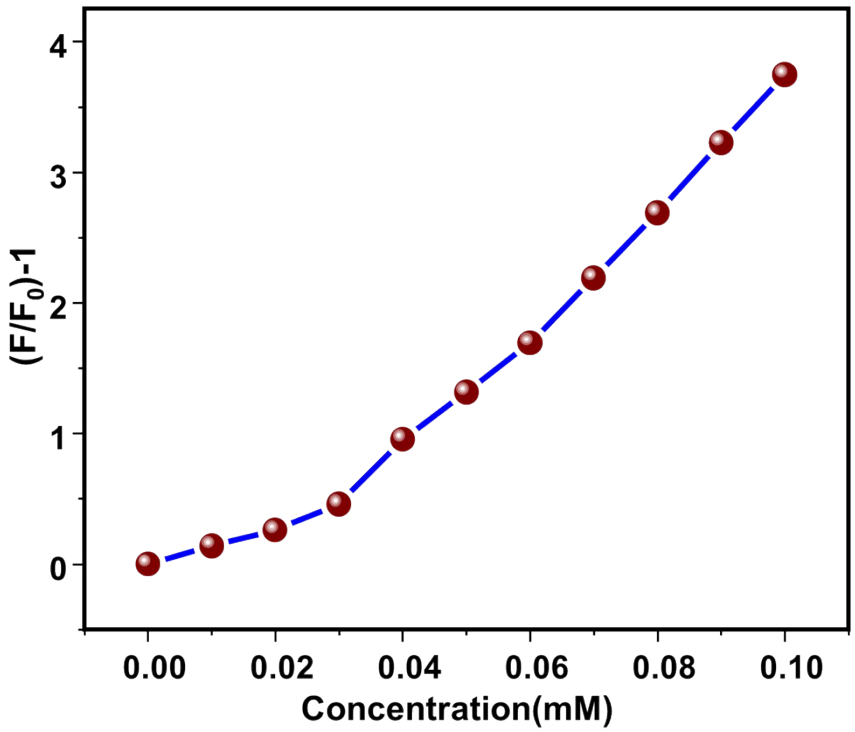

Figure S46. The nonlinear nature of the plot for 1 mM ADP solution (total concentration 0–0.1 mM, 0 µL -200 µL).

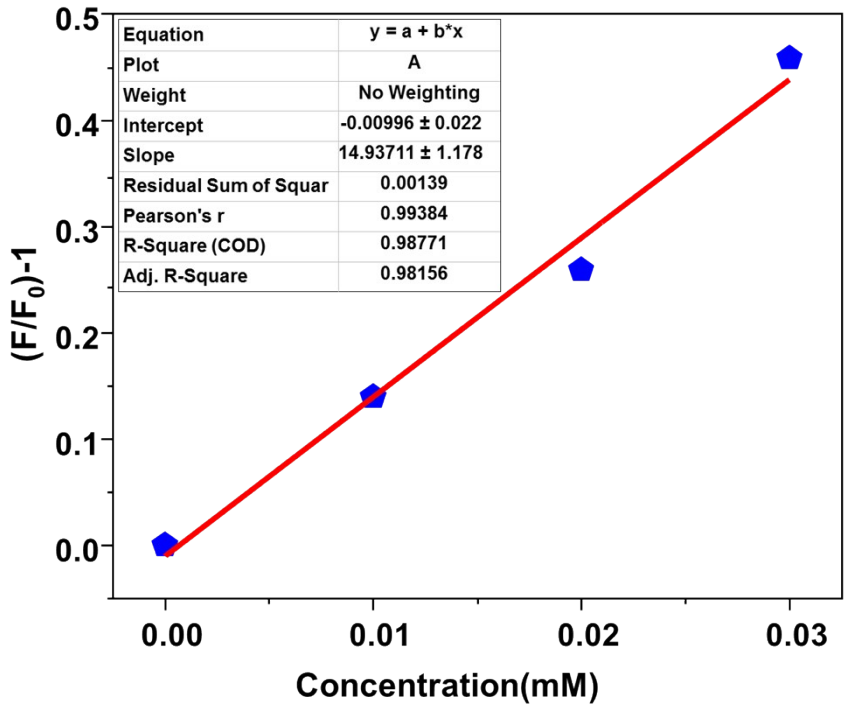

Figure S47. Fluorescence enhancement coefficient (EC) determination plot for of **2a**. The relative fluorescence intensity (F/F_0)-1 is linear with ADP concentration in the range of 0–0.03 mM.

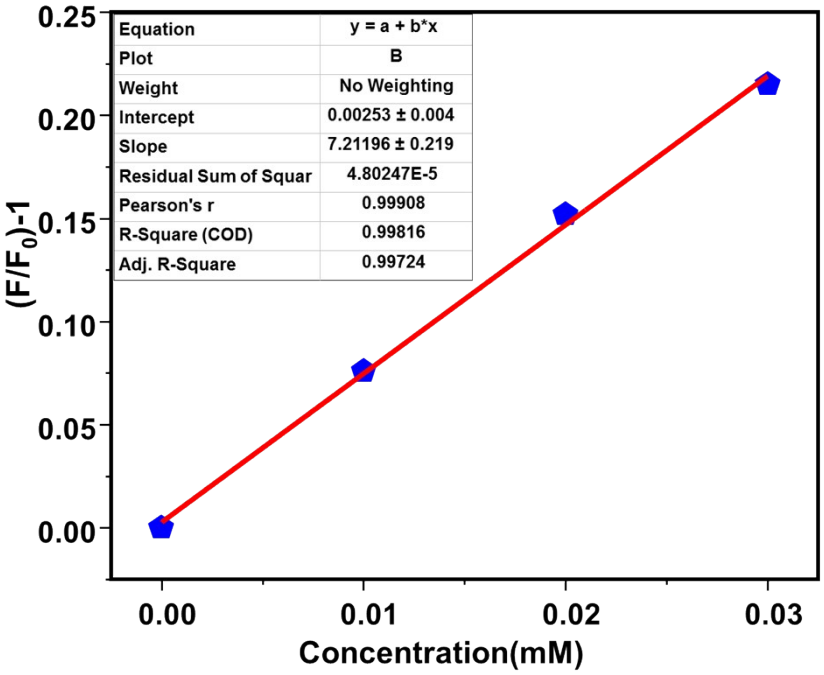

Figure S48. Fluorescence enhancement coefficient (EC) determination plot for of **2a**. The relative fluorescence intensity (F/F_0)-1 is linear with ATP concentration in the range of 0–0.03 mM.

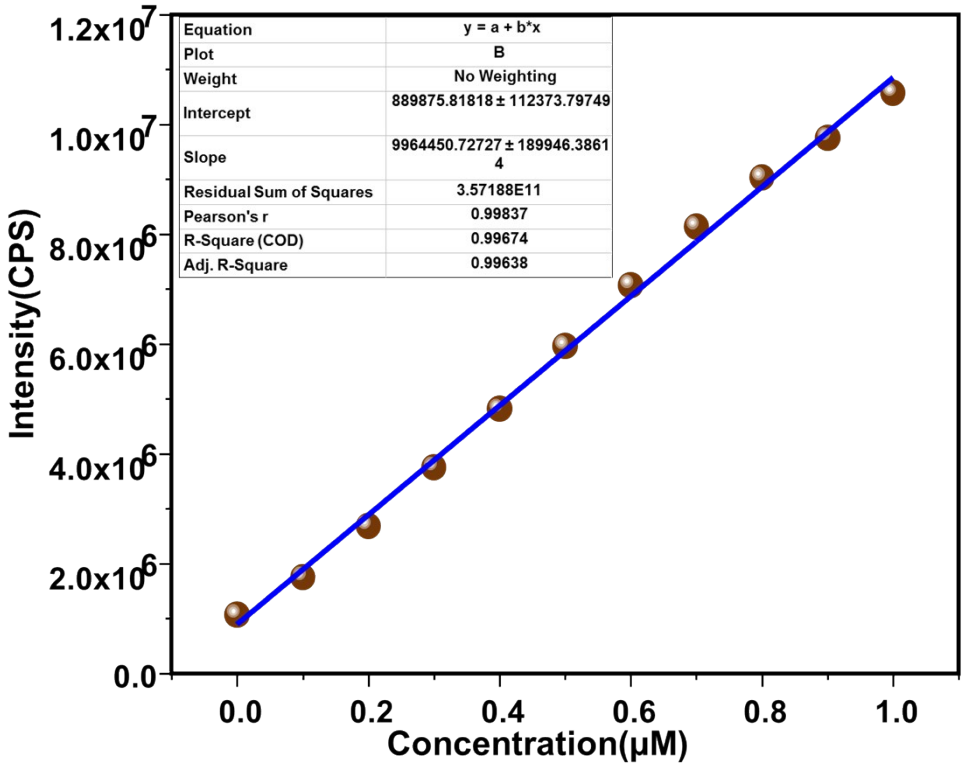

Figure S49. Linear region of fluorescence intensity of **2a** upon addition of (0 – 200 μL, 10 μM stock solution).

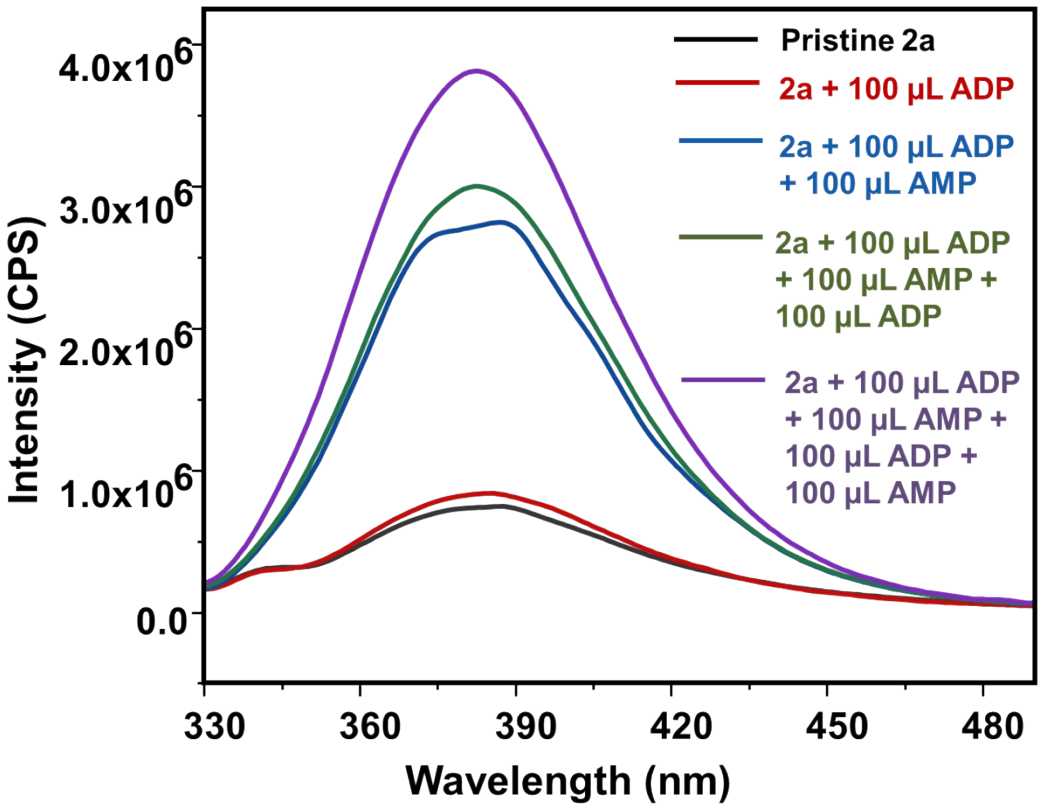

Figure S50. Change in fluorescence spectrum of **2a**, upon simultaneous addition of AMP in presence of ADP (0 µL -400 µL, 100 µL alternating addition of each analyte).

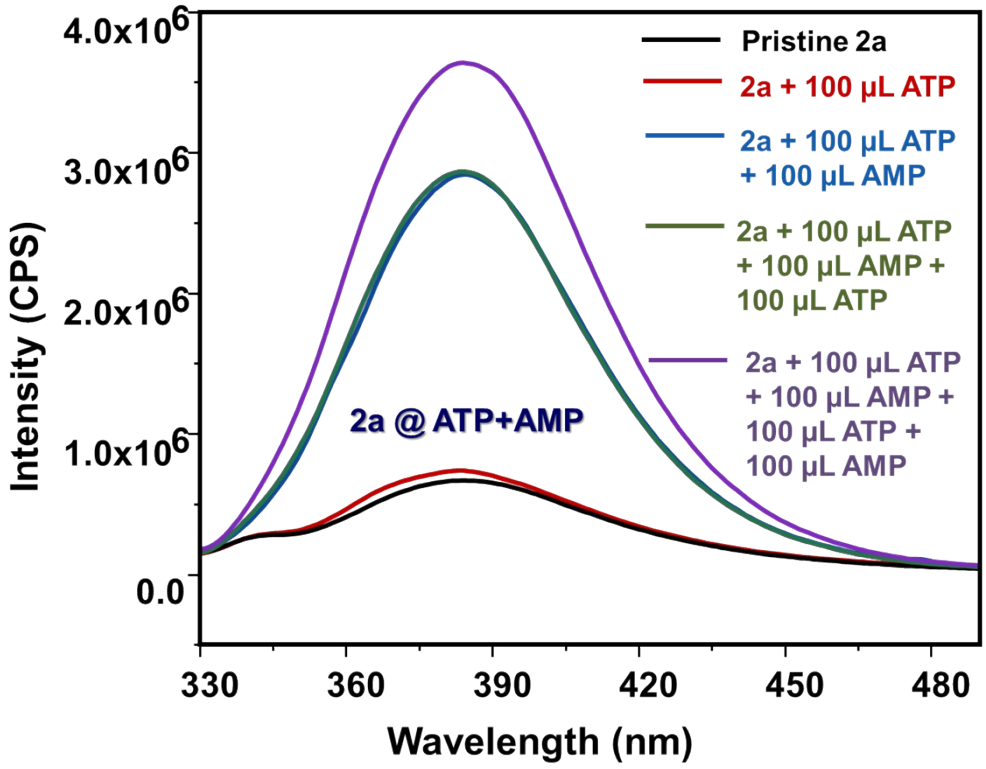

Figure S51. Change in fluorescence spectrum of **2a**, upon simultaneous addition of AMP in presence of ATP (0 µL -400 µL, 100 µL alternating addition of each analyte).

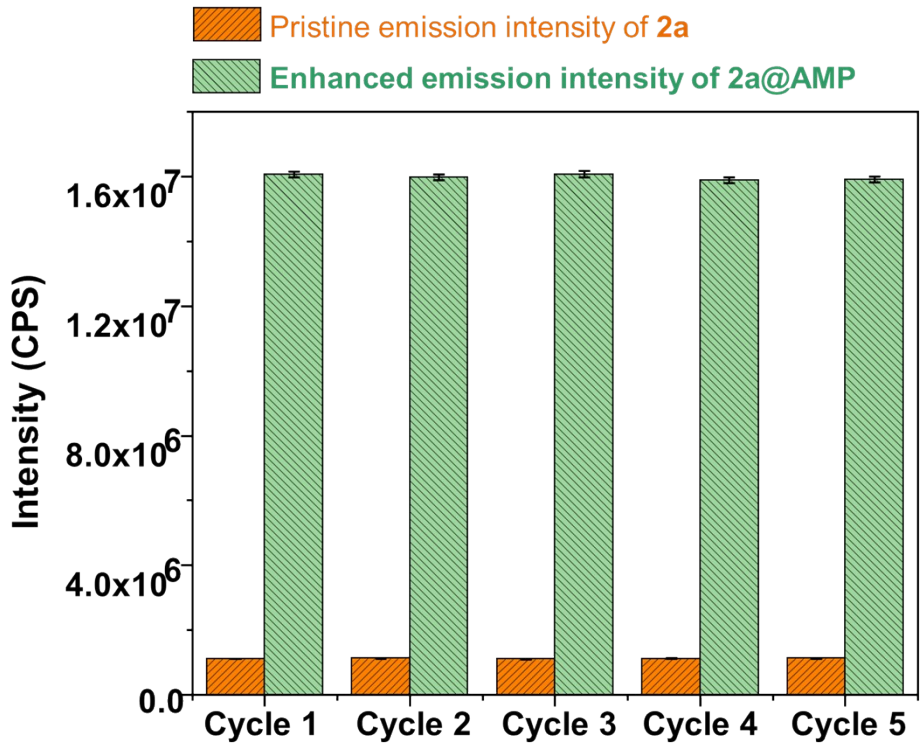

Figure S52. Reproducibility of enhancing efficiency of **2a** towards 1 mM AMP solution up to 5 cycles.

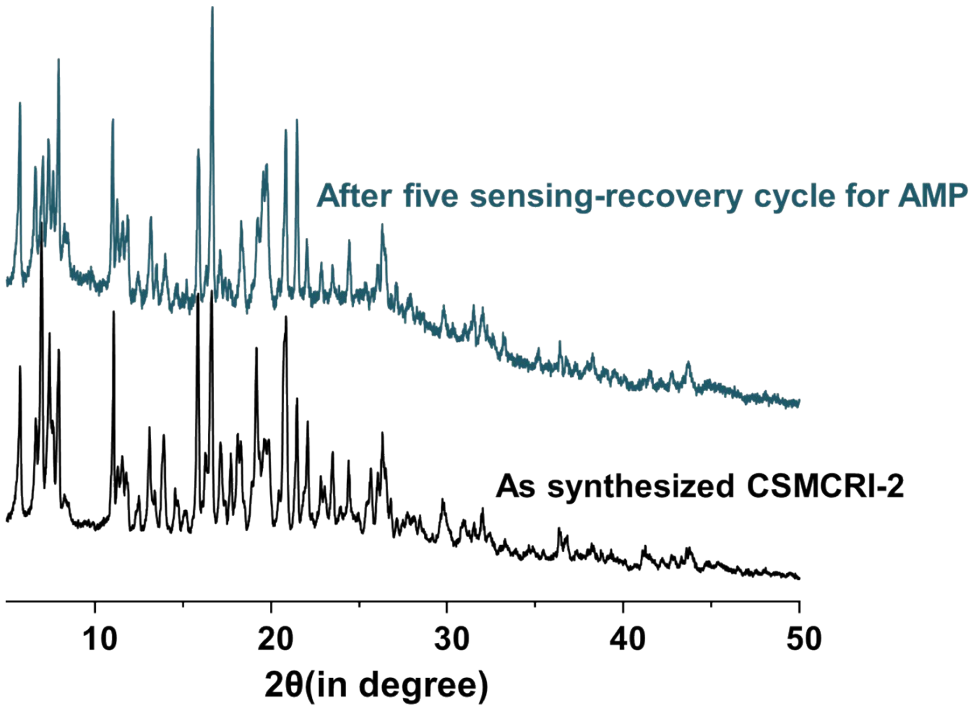

Figure S53. PXRD curves of **2a** after five sensing recovery cycles for AMP (1 mM), showing that structural integrity of the framework is maintained.

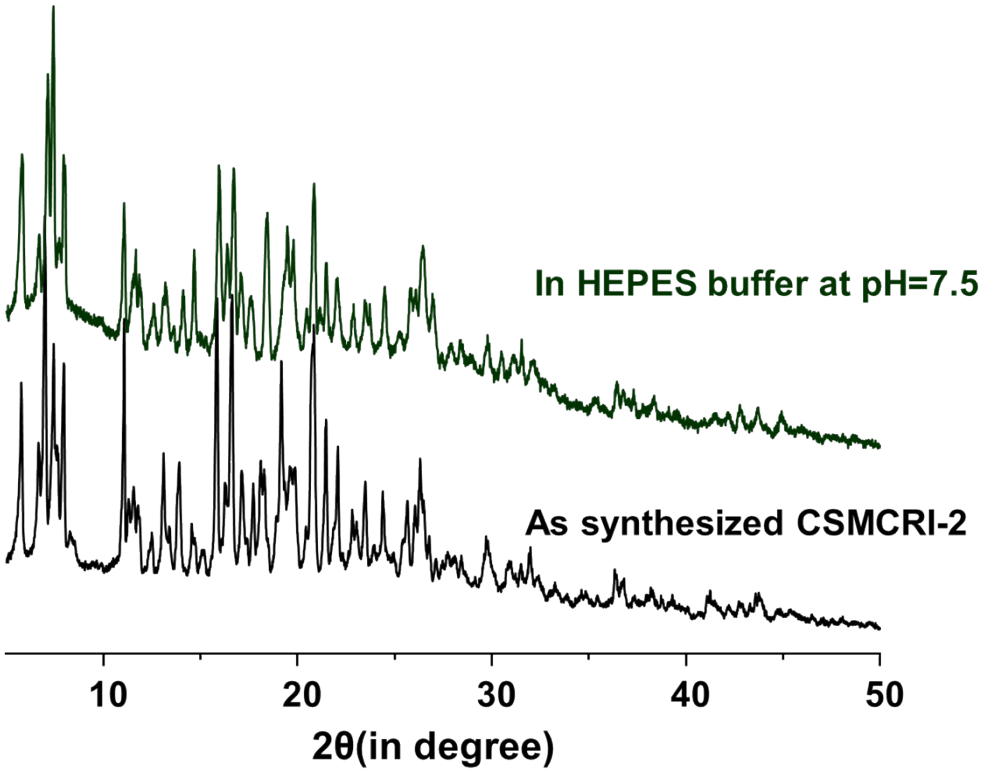

Figure S54. PXRD curves of **2a** in presence of HEPES buffer (pH=7.5), showing that structural integrity of the framework is maintained.

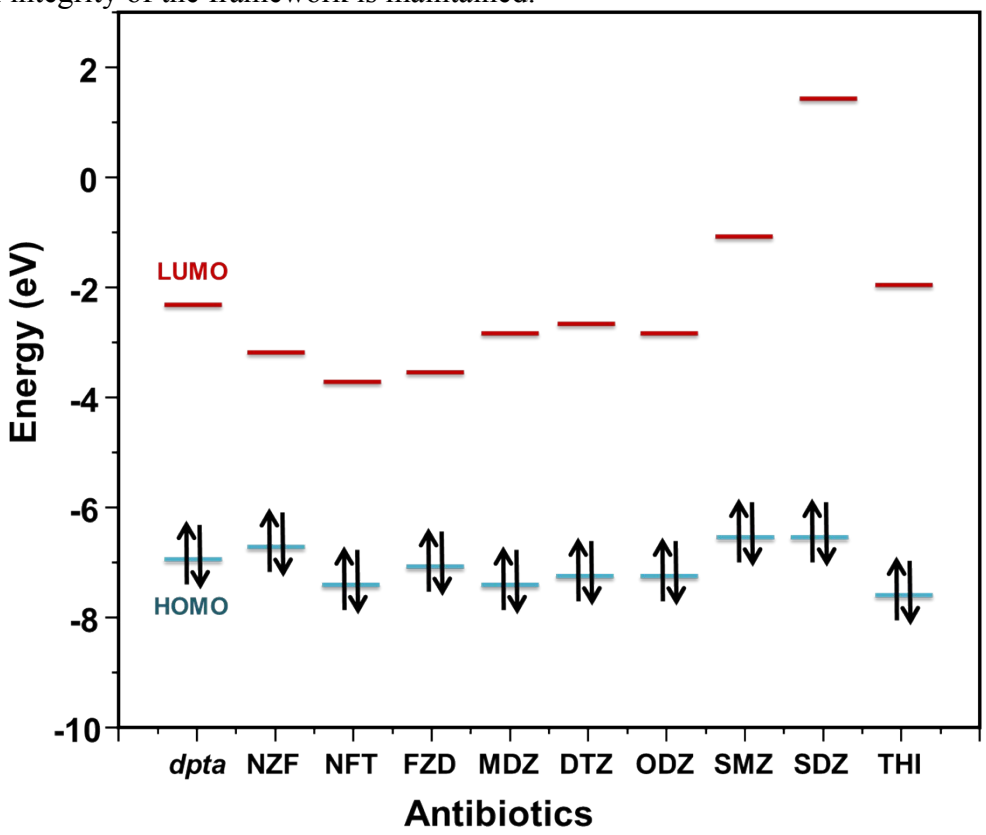

Figure S55. HOMO–LUMO energies for linker *dpta* along with all the studied antibiotics.

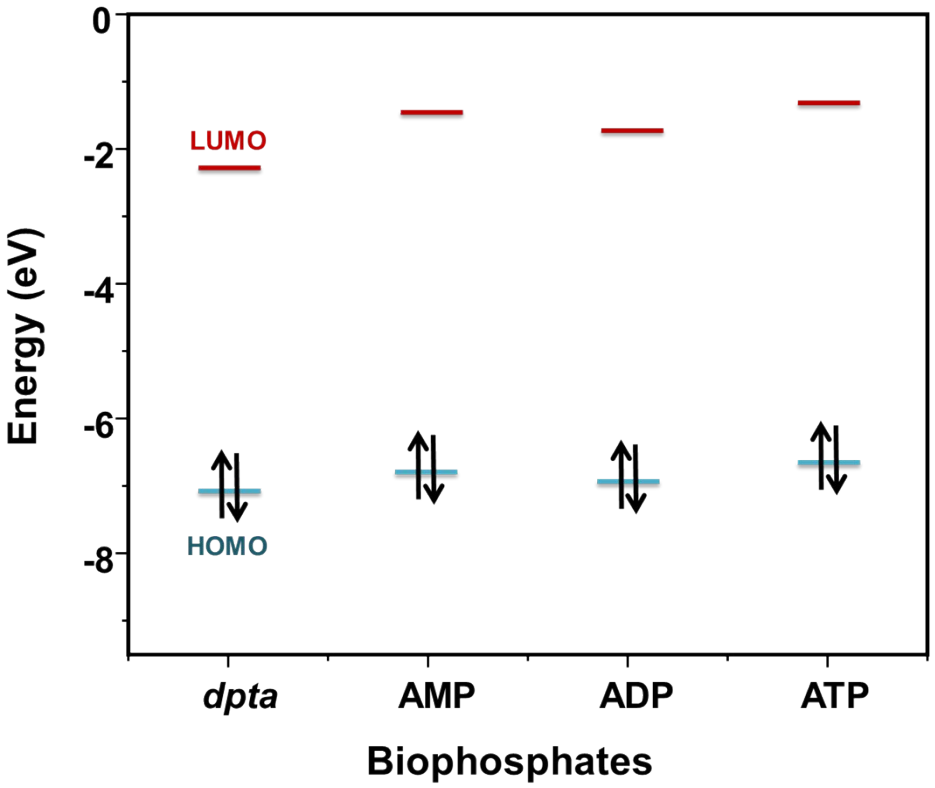

Figure S56. HOMO–LUMO energies for linker *dpta* along with all the studied biophosphates.

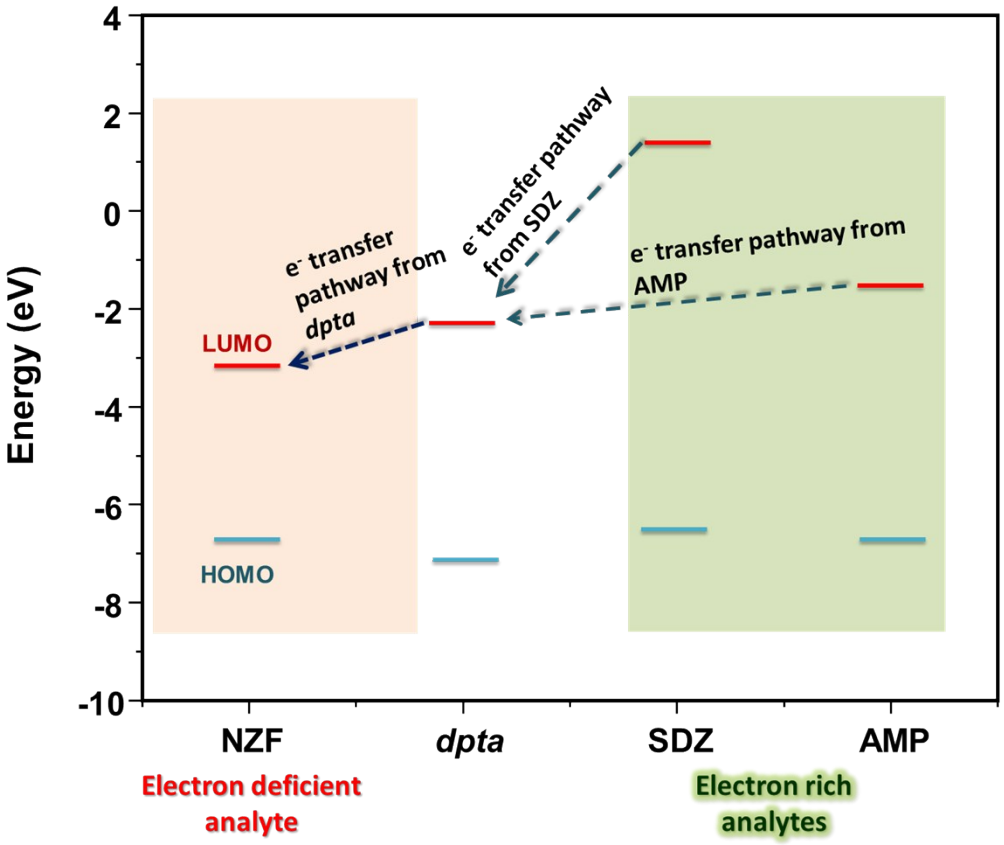

Figure S57. Schematic presentation of charge transfer pathway between **2a** and selective analytes.

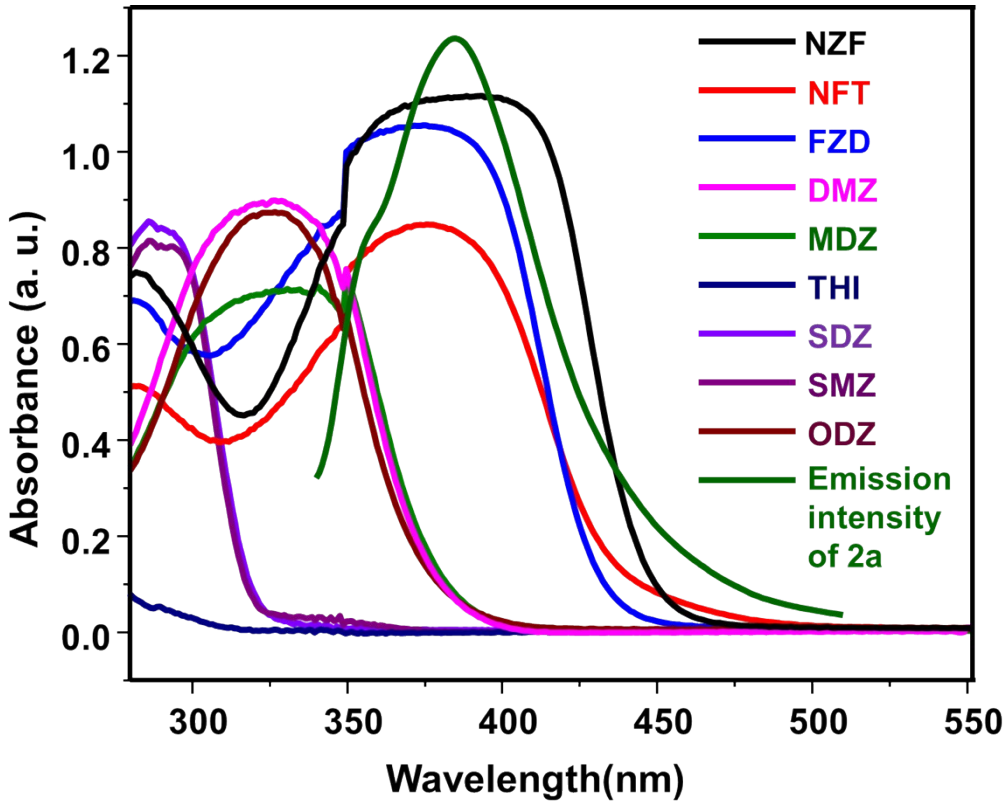

Figure S58. Spectral overlap between the absorption spectra of all the antibiotics and emission spectrum of **2a**.

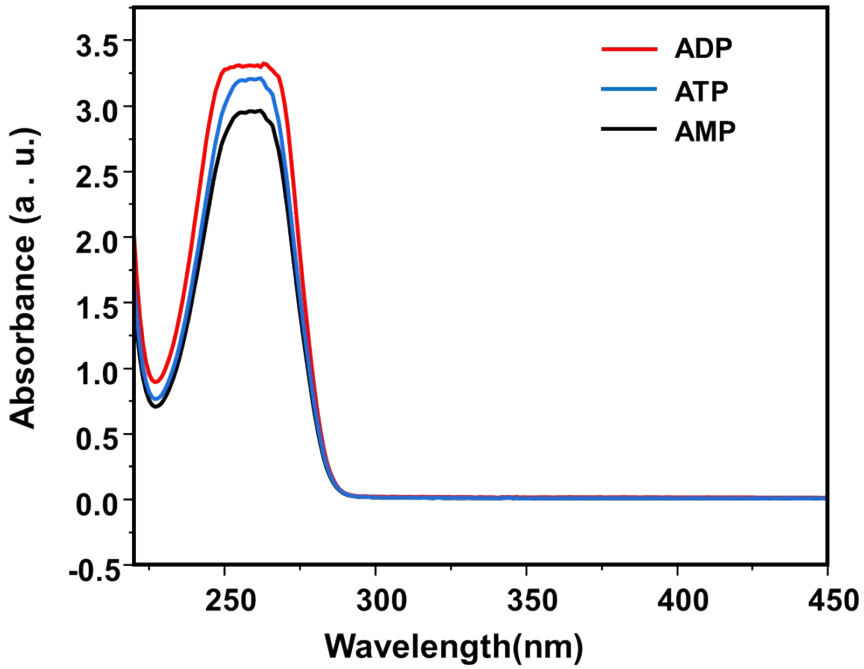

Figure S59. Absorption spectra of the studied biophosphates.

Table S1. Crystal data and refinement parameters

Identification code	**CSMCRI-2**
Empirical formula	$C_{52}H_{54}N_{14}O_{12}Zn_2$
Crystal color and shape	Orange block
Formula weight	1197.83

Temperature/K	150.15
Crystal system	triclinic
Space group	*P-1*
a/Å	13.657(2)
b/Å	15.099(3)
c/Å	17.129(3)
α/°	69.483(2)
β/°	71.932(2)
γ/°	74.038(2)
Volume/Å^3	3089.6(9)
Z	2
ρ_{calc} /g/cm^3	1.288
μ/mm^{-1}	0.843
F(000)	1240.0
Crystal size/mm^3	0.4 × 0.23 × 0.1
Radiation	MoKα (λ = 0.71073)
2Θ range for data collection/°	2.614 to 56.252
Index ranges	-18 ≤ h ≤ 17, -19 ≤ k ≤ 19, -22 ≤ l ≤ 22
Reflections collected	24010
Independent reflections	13053 [R_{int} = 0.0341, R_{sigma} = 0.0633]
Data/restraints/parameters	13053/0/738
Goodness-of-fit on F^2	1.061
Final R indexes [I>=2σ (I)]	R_1 = 0.0652, wR_2 = 0.1780
Final R indexes [all data]	R_1 = 0.0876, wR_2 = 0.1887
Largest diff. peak/hole / e Å^{-3}	0.86/-0.73

Table S2. Calculation of standard deviation of fluorescence intensity and limit of detection for **2a** towards SDZ

Blank Readings (2a)	**Fluorescence Intensity(CPS)**
Reading 1	729437
Reading 2	705430
Reading 3	673160
Reading 4	669690
Reading 5	643120
Standard Deviation (σ)	33604
Slope from Graph (K)	1.54 x 10^6 μM^{-1}
Detection limit ($3\sigma/K$)	0.065 μM / **65nM**
Limit of Detection (LOD)	0.05 ppm / **50 ppb**

Table S3. Calculation of standard deviation of fluorescence intensity and limit of detection for **2a** towards NZF

Blank Readings (2a)	**Fluorescence Intensity(CPS)**
Reading 1	729437
Reading 2	705430
Reading 3	673160
Reading 4	669690
Reading 5	643120
Standard Deviation (σ)	33604
Slope from Graph (K)	142914 μM^{-1}
Detection limit ($3\sigma/K$)	0.7 μM
Limit of Detection (LOD)	**0.63 ppm**

Table S4. Calculation of standard deviation of fluorescence intensity and limit of detection for **2a** towards AMP

Blank Readings (2a)	**Fluorescence Intensity(CPS)**
Reading 1	729437
Reading 2	705430
Reading 3	673160
Reading 4	669690
Reading 5	643120
Standard Deviation (σ)	33604
Slope from Graph (K)	9.96×10^6 μM^{-1}
Detection limit ($3\sigma/K$)	0.010μM / **10nM**
Limit of Detection (LOD)	0.009 ppm / **9 ppb**

Table S5. HOMO and LUMO energy levels of different antibiotics calculated by density functional theory (DFT) at B3LYP/6-311++G** accuracy level, using Gaussian 09 package of programs [9]

Analytes	HOMO (eV)	LUMO (eV)	Energy gap (eV)
NZF	-6.79	-3.14	3.65
NFT	-7.37	-3.66	3.71
FZD	-7.15	-3.49	3.66
MDZ	-7.34	-2.85	4.49
DTZ	-7.30	-2.76	4.54
ODZ	-7.32	-2.89	4.43
SMZ	-6.53	-1.17	5.36
SDZ	-6.59	-1.46	5.13
THI	-7.70	-2.00	5.70
MOF constituting linker (*dpta*)	-7.04	-2.32	4.72

Table S6. HOMO and LUMO energy levels of different biophosphates calculated by density functional theory (DFT) at B3LYP/6-311++G** accuracy level, using Gaussian 09 package of programs

Analytes	HOMO (eV)	LUMO (eV)	Energy gap (eV)
AMP	-6.84	-1.53	5.31
ADP	-7.00	-1.69	5.31
ATP	-6.67	-1.40	5.27
MOF constituting linker (*dpta*)	-7.04	-2.32	4.72

Table S7. A comparison of enhancement in fold / enhancement constant, of various luminescent MOFs used for detection of analytes in literature

Sl. No.	MOF/Coordination polymer	Analyte used for sensing	Enhancement in fold/ enhancement constant	Ref.
1.	PCN-222	Cu(II) ion	10 fold	Chem. Mater. 2016, 28, 6698−6704
2.	$\{Cd_3(L_1)(bipy)_2 \cdot 4DMA\}_n$	Benzene	8 fold	Mater. Horiz., 2015, 2, 245–251
3.	Fe-MIL-88/H_2O_2	Biothiols	5 fold	Analyst, 2015, 140, 8201–8208
4.	$Zr(TBAPy)_5(TCPP)$	H_2S gas	$1.37\times 10^4\ M^{-1}$	Small 2018, *14*, 1703822
5.	1-N_3	H_2S gas	16 fold	Sci. Rep., 2014, 4, 7053
6.	$[Eu_2(L_2)_3(H_2O)_4]\cdot 3DMF$	DMF Vapor	8 fold	Angew. Chem. Int. Ed. 2013, 52, 710 –713
7.	$[Co(OBA)\text{-}(DATZ)_{0.5}(H_2O)]$	Al(III) ion	6.3 fold	Inorg. Chem. 2015, 54, 6373−6379
8.	bio-MOF-1 Ↄ DAAC	CN^- ion	17 fold	Chem. Commun., 2017, 53, 1253--1256
9.	CSMCRI-2	Sulfadiazine antibiotic	29.6 fold /$7.06\times 10^5\ M^{-1}$	This work

L_1: (hexa[4-(carboxyphenyl)oxamethyl]-3-oxapentane acid), TBAPy : 1,3,6,8-tetra (4-carboxylphenyl) pyrene, TCPP : tetrakis(4-carboxyphenyl)porphyrin, L_2: 2',5'-bis(methoxymethyl)-[1,1':4',1''-terphenyl]-4,4''-dicarboxylate, OBA: 4,4'-oxybis(benzoic acid), DATZ: 3,5-diamino-1,2,4-triazole, DAAC: 3,6-diaminoacridinium cation

Table S8. A comparison of quenching constant, their LOD, of various luminescent MOFs used for detection of NZF

Sl. No.	MOF	Quenching constant (M^{-1})	Limit of Detection	Medium Used	Ref.
1.	BUT-12 BUT-13	1.1×10^5 7.5×10^4	58 ppb 90 ppb	Water	J. Am. Chem. Soc. 2016, 138, 6204−6216
2.	$[Cd_2(L_1)(BPDC)_2]\cdot DMF\cdot 9H_2O$	1.33×10^5	60 ppb	DMF	J. Mater. Chem. A, 2017, 5, 15797–15807
3.	$\{(Me_2NH_2)[In(L_2)]\cdot 2.5DEF\}_n$	6.38×10^4	0.2 ppm	Water	Anal. Chem. 90, 3, 1516-1519
4.	$[Zn_4O(L_3)_3]$	NA	0.1 ppm	Water	J. Mater. Chem. C, 2018, 6, 2983-2988
5.	$[Mg_2(L_4)_2(H_2O)_3]\cdot 5DMA\cdot 5H_2O$	9.0×10^4	108 ppb	DMF	Inorg. Chem., 2018, 57 (21), pp 13330–13340
6.	$[Zn_3(L_5)_{1.5}(L_6)_3]\cdot(DMF)_{5.9}\cdot(H_2O)_{1.05}$	8.75×10^4	0.8 ppm	DMF	ACS Appl. Mater. Interfaces, 2019, 11 (9), pp 9042–9053
7.	CSMCRI-2	1.30×10^5	0.63 ppm	DMF	This work
L_1: L_1: N^1-(4-(1*H*-1,2,4-triazole-1-yl)benzyl)-N^1-(2-aminoethyl)ethane-1,2-diamine, BPDC: biphenyl-4,4′-dicarboxylic acid, L2: 5-(2,6-bis(4-carboxyphenyl) pyridin-4-yl) isophthalic acid, L_3: 4,4′-(1,2-diphenylethene-1,2-diyl)dibenzoic acid, L_4 : 4,4′-(4-aminopyridine-3,5-diyl)dibenzoic acid, L_5 : meso-α,β-di(4-pyridyl) glycol, L_6 : Azobenzene-4,4'-dicarboxylic Acid					

References:

1. L. Cheng, W. X. Zhang, B. H. Ye, J. B. Lin, X. M. Chen, *Inorg. Chem.* **2007**, *46*, 1135.

2. SAINT+, version 6.02; Bruker AXS: Madison, WI, **1999**.

3. G. M. Sheldrick, *SADABS*, Empirical Absorption Correction Program; University of Göttingen: Göttingen, Germany, **1997**.

4. *XPREP*, version 5.1; Siemens Industrial Automation Inc.: Madison, WI, **1995**.

5. G. M. Sheldrick, *SHELXTL* Reference Manual: version 5.1; Bruker AXS: Madison, WI, **1997**.

6. G. M. Sheldrick, *SHELXL*-2014/7; University of Göttingen: Göttingen, Germany.

7. A. L. Spek, PLATON; The University of Utrecht: Utrecht, The Netherlands, **1999**.

8. http://www.topos.ssu.samara.ru; V. A. Blatov, IUCr CompComm News letter **2006**, 7, 4.

9. M. J. Frisch, G. W. Trucks, H. B. Schlegel, G. E. Scuseria, M. A. Robb, J. R. Cheeseman, G. Scalmani, V. Barone, B. Mennucci, G. A. Petersson, H. Nakatsuji, M. Caricato, X. Li, H. P. Hratchian, A. F. Izmaylov, J. Bloino, G. Zheng, J. L. Sonnenberg, M. Hada, M. Ehara, K. Toyota, R. Fukuda, J. Hasegawa, M. Ishida, T. Nakajima, Y. Honda, O. Kitao, H. Nakai, T. Vreven, J. A. Montgomery, Jr., J. E. Peralta, F. Ogliaro, M. Bearpark, J. J. Heyd, E. Brothers, K. N. Kudin, V. N. Staroverov, R. Kobayashi, J. Normand, K. Raghavachari, A. Rendell, J. C. Burant, S. S. Iyengar, J. Tomasi, M. Cossi, N. Rega, J. M. Millam, M. Klene, J. E. Knox, J. B. Cross, V. Bakken, C. Adamo, J. Jaramillo, R. Gomperts, R. E. Stratmann, O. Yazyev, A. J. Austin, R. Cammi, C. Pomelli, J. W. Ochterski, R. L. Martin, K. Morokuma, V. G. Zakrzewski, G. A. Voth, P. Salvador, J. J. Dannenberg, S. Dapprich, A. D. Daniels, Ö. Farkas, J. B. Foresman, J. V. Ortiz, J. Cioslowski, D. J. Fox, Gaussian 09; Revision D.01, Gaussian, Inc: Wallingford, CT, **2013**.